Article

Cell

Distinct Dopamine Receptor Pathways Underlie the Temporal Sensitivity of Associative Learning

Graphical Abstract

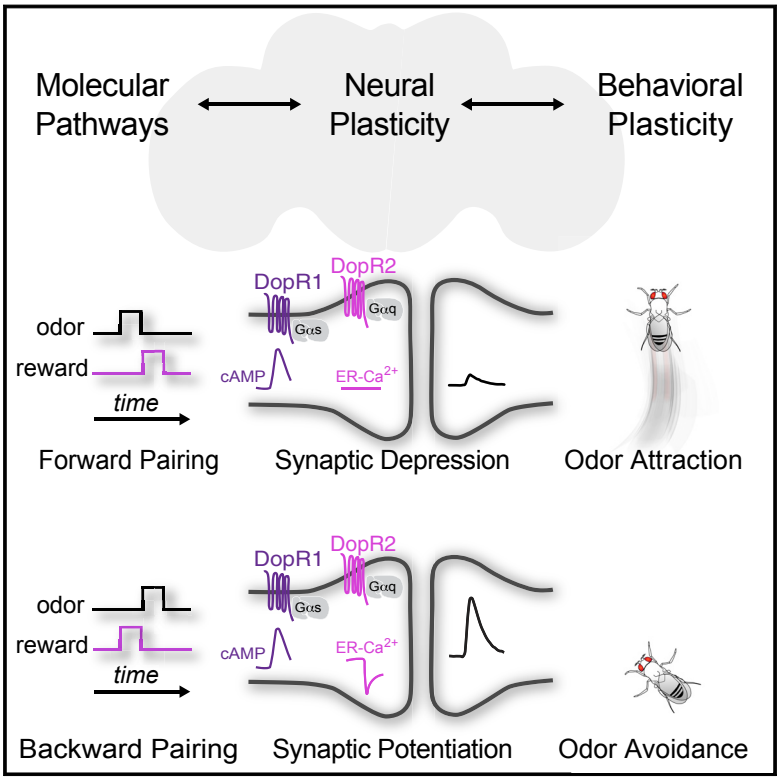

Highlights

- The timing of odor and dopaminergic reinforcement instructs opposing associations
- Bidirectional plasticity in the mushroom body correlates with these learned behaviors
- Distinct DopR1 and DopR2 signaling cascades exhibit different temporal sensitivity
- Behavioral and neural plasticity depend on the balance of DopR1 and DopR2 signaling

Authors

Annie Handler, Thomas G.W. Graham, Raphael Cohn, ..., Jianzhi Zeng, Yulong Li, Vanessa Ruta

Correspondence

ruta@rockefeller.edu

In Brief

Olfactory associations are formed and updated on a trial-by-trial basis depending on the timing of the odor presentation and reinforcement mediated by two dopamine receptor signaling pathways that play opposing roles in directing synaptic and behavioral plasticity in *Drosophila*.

Handler et al., 2019, Cell *178*, 60–75
June 27, 2019
https://doi.org/10.1016/j.cell.2019.05.040

CellPress

Cell

Article

Distinct Dopamine Receptor Pathways Underlie the Temporal Sensitivity of Associative Learning

Annie Handler,[1] Thomas G.W. Graham,[1] Raphael Cohn,[1] Ianessa Morantte,[1] Andrew F. Siliciano,[1] Jianzhi Zeng,[2] Yulong Li,[2] and Vanessa Ruta[1,3,*]

[1]Laboratory of Neurophysiology and Behavior, The Rockefeller University, New York, NY 10065, USA

[2]State Key Laboratory of Membrane Biology, Peking University School of Life Sciences, PKU-IDG/McGovern Institute for Brain Research, Peking-Tsinghua Center for Life Sciences, 100871 Beijing, China

[3]Lead Contact

*Correspondence: ruta@rockefeller.edu

https://doi.org/10.1016/j.cell.2019.05.040

SUMMARY

Animals rely on the relative timing of events in their environment to form and update predictive associations, but the molecular and circuit mechanisms for this temporal sensitivity remain incompletely understood. Here, we show that olfactory associations in *Drosophila* can be written and reversed on a trial-by-trial basis depending on the temporal relationship between an odor cue and dopaminergic reinforcement. Through the synchronous recording of neural activity and behavior, we show that reversals in learned odor attraction correlate with bidirectional neural plasticity in the mushroom body, the associative olfactory center of the fly. Two dopamine receptors, DopR1 and DopR2, contribute to this temporal sensitivity by coupling to distinct second messengers and directing either synaptic depression or potentiation. Our results reveal how dopamine-receptor signaling pathways can detect the order of events to instruct opposing forms of synaptic and behavioral plasticity, allowing animals to flexibly update their associations in a dynamic environment.

INTRODUCTION

To survive in a complex environment, animals must learn which sensory cues are predictive of reward or punishment and which are irrelevant. Associative circuits must therefore be sensitive to the relative timing and order of events in the environment, as this allows animals to infer the meaningful relationships between cues and outcomes.

Neural circuits involved in associative learning integrate sensory signals with rewarding or punishing reinforcement cues, frequently encoded by neuromodulatory dopaminergic neurons (DANs; Aso et al., 2014a; Bromberg-Martin et al., 2010; Lerner et al., 2015; Schultz et al., 1997; Waddell, 2016). This convergence of sensory and reinforcement pathways is thought to induce the circuit plasticity that underlies adaptive changes in behavior (Owald and Waddell, 2015; Pignatelli and Bonci, 2015; Surmeier et al., 2009). A strict temporal relationship between a sensory signal, such as an odor, and a reinforcement is required to drive learning: in order for the odor to predict an ensuing positive or negative outcome, it must consistently precede the reinforcement in time. This tight temporal contiguity represents a core principle of classical conditioning (Kandel et al., 1983; Mauk and Donegan, 1997; Pavlov, 2010; Rescorla, 1988; Tully and Quinn, 1985), as it permits animals to learn about the causal structure of the world around them.

Behavioral experiments in diverse species, from flies to humans, indicate that animals can form opposing associations with a sensory stimulus depending on its timing relative to a reinforcement cue (Gerber et al., 2014). *Drosophila*, for example, can form either negative or positive associations with an odor depending on whether the odor precedes or follows an aversive reinforcement during conditioning (Aso and Rubin, 2016; König et al., 2018; Tanimoto et al., 2004). This capacity suggests that the mushroom body, the associative olfactory center of *Drosophila*, is sensitive to the temporal ordering of an odor stimulus and a reinforcement, allowing flies to endow odors with distinct meaning depending on whether they predict a reinforcement or are associated with its termination. Such sensitivity may also provide a mechanism to overwrite inaccurate or obsolete associations as the temporal structure of the olfactory environment changes. Yet while the modulatory mechanisms for memory formation in the mushroom body have been extensively investigated (Heisenberg, 2003; Hige, 2018; Owald and Waddell, 2015), the underlying molecular or circuit basis for this temporal sensitivity remains incompletely understood.

In the mushroom body, odor identity is encoded by the activity of sparse ensembles of Kenyon cells (KCs) (Campbell et al., 2013; Turner et al., 2008) whose parallel axons bundle together to form output lobes. The mushroom body lobes are tiled by discrete anatomic compartments defined by the segregated axons of a subset of DANs and the dendrites of one or two mushroom body output neurons (MBONs) (Aso et al., 2014a; Tanaka et al., 2008). Positive and negative reinforcements are conveyed by distinct DANs that innervate different compartments, with the protocerebral posterior lateral (PPL) DANs carrying predominantly aversive signals (Aso et al., 2010, 2012; Claridge-Chang et al., 2009; Mao and Davis, 2009) and the protocerebral anterior medial (PAM) DANs conveying reward information (Burke et al., 2012; Liu et al., 2012; Yamagata et al., 2015). As a consequence of this compartmentalized organization, DANs can independently tune the strength of KC-MBON synapses within each compartment (Cohn et al., 2015; Hige et al., 2015; Owald et al.,

2015; Séjourné et al., 2011), reweighting the net activity of the output population to bias an animal's attraction to an odor through learning.

Here, we combine high-resolution behavioral analysis with functional imaging to investigate how the *Drosophila* mushroom body detects the precise temporal ordering of events to extract meaningful relationships from the environment. We show that flies can write opposing olfactory associations on a trial-by-trial basis depending on the relative timing of odor cues and a dopaminergic reinforcement. Using a closed-loop olfactory system to monitor neural activity as an animal navigates in a virtual olfactory environment, we reveal that bidirectional plasticity in KC-MBON signaling correlates with the emergence of these learned behaviors. Furthermore, we show that the temporal specificity of this circuit relies on two dopamine receptors that couple to distinct intracellular signaling cascades and play opposing roles in regulating KC-MBON synaptic strength. Loss of either receptor renders the synapses of the mushroom body capable of only unidirectional plasticity, preventing this behavioral flexibility. By examining dopamine receptor second-messenger signaling and neural and behavioral plasticity on the same timescales, our experiments reveal how biochemical pathways confer temporal sensitivity to this circuit, allowing animals to form and maintain accurate predictions in a complex and changing environment.

RESULTS

Rapid and Repeated Updating of Olfactory Associations

To explore how *Drosophila* adapt to changes in the temporal structure of their environment, we developed methods to monitor the olfactory preferences of flies while precisely varying the timing of odor stimuli and dopaminergic reinforcement. An advantage of this assay over traditional paradigms, like the T-maze, is that it allows for repeated training and testing of the same individuals over several hours, permitting longitudinal examination of how odor attraction is altered in response to ongoing experience. We placed a cohort of 4–7 flies in a small chamber (Figure S1A) in constant laminar airflow and analyzed their walking trajectories in response to a brief pulse of the appetitive odor, apple cider vinegar (ACV) (see Video S1). A common navigational strategy many animals employ is to reorient and increase their upwind velocity when they encounter an attractive olfactory plume (Álvarez-Salvado et al., 2018; Bell and Wilson, 2016; Steck et al., 2012). Likewise, naive flies exhibited robust upwind tracking of ACV, evident from visualizing the trajectories of individual animals (Figure 1B) or measuring the upwind velocity of the population's center of mass within the chamber (Figure 1C).

We began by asking whether we could suppress the innate attraction to ACV by pairing it with optogenetic activation of the PPL DANs that encode punitive cues and are sufficient to drive aversive memory formation (Aso et al., 2010, 2012; Claridge-Chang et al., 2009; König et al., 2018) (Figures 1A and 1B). We used an intersectional genetic strategy (Aso et al., 2014a) to selectively express the opsin, CsChrimson, in a subset of PPL neurons innervating six compartments of the mushroom body, allowing for temporally precise, light-evoked dopaminergic reinforcement. After just a single forward conditioning trial, in which the ACV stimulus preceded the onset of PPL activation, flies showed significantly reduced odor tracking (Figures 1B, 1C, and S1B). This aversive conditioning resulted in both fewer flies tracking upwind in response to the odor and lower walking speeds for those that did track (Figures 1B, 1C, and S2A–S2J).

The attenuated attraction to ACV after forward conditioning persisted for tens of minutes with little erosion due to passive decay (Figure S1B), underscoring that a single aversive reinforcement can drive lasting behavioral modulation. However, if animals subsequently experienced a single backward conditioning trial, in which ACV now followed PPL stimulation, the weakened attraction was immediately reversed, rendering flies strongly attracted to the odor again (Figures 1B, 1C, and S1C). Interleaving forward and backward pairing reliably modulated the animals' attraction to ACV for 50 conditioning trials by reversibly modifying multiple facets of tracking behavior (Figures S2A–S2J). Plotting the upwind displacement of animals over time generated a saw-tooth pattern, as their upwind tracking was alternately suppressed or enhanced with each conditioning trial (Figures 1D and 1F). This systematic modulation was not evident in control animals, in which light alone had a minimal effect on behavior (Figures S1D and S1E). Flies therefore have the capacity to write and update odor associations on a trial-by-trial basis as the predictive value of an odor changes. This reversal in odor tracking with forward and backward conditioning parallels previous observations that animals will avoid odors that predict punishment but become attracted to odors associated with its termination (Aso and Rubin, 2016; König et al., 2018; Tanimoto et al., 2004).

We next asked whether olfactory associations could be similarly modulated via activation of the PAM cluster of DANs responsive to rewarding stimuli that drive appetitive learning (Burke et al., 2012; Liu et al., 2012; Yamagata et al., 2015; Figure 1A). Forward pairing of ACV with PAM activation modestly enhanced the upwind tracking of ACV in naive animals. However, a single backward conditioning trial robustly suppressed odor tracking, independently of whether animals had been previously conditioned or not (Figures 1E and S1F). This suggests that backward pairing, in which the odor becomes associated with the cessation of reward, instructs the formation of an aversive memory that can both suppress naive attraction and overwrite a prior appetitive association. As with PPL conditioning, alternating forward and backward pairing of ACV with PAM activation modulated odor attraction with each trial, enhancing upwind tracking after forward pairing and suppressing tracking after backward pairing (Figures 1E, 1G, and S2A–S2J). Thus, both PAM and PPL DANs are sufficient to bidirectionally modify behavior such that activation of either dopaminergic population can produce appetitive or aversive associations depending on whether the odor precedes or follows the reinforcement in time.

A learned olfactory association can be weakened if an animal encounters the odor in the absence of the anticipated reinforcement or the reinforcement in the absence of the conditioned odor, violating the expected contingency between these cues (Aso and Rubin, 2016; Berry et al., 2012; Bouton, 2002; Felsenberg et al., 2017). However, in our assay interleaving forward

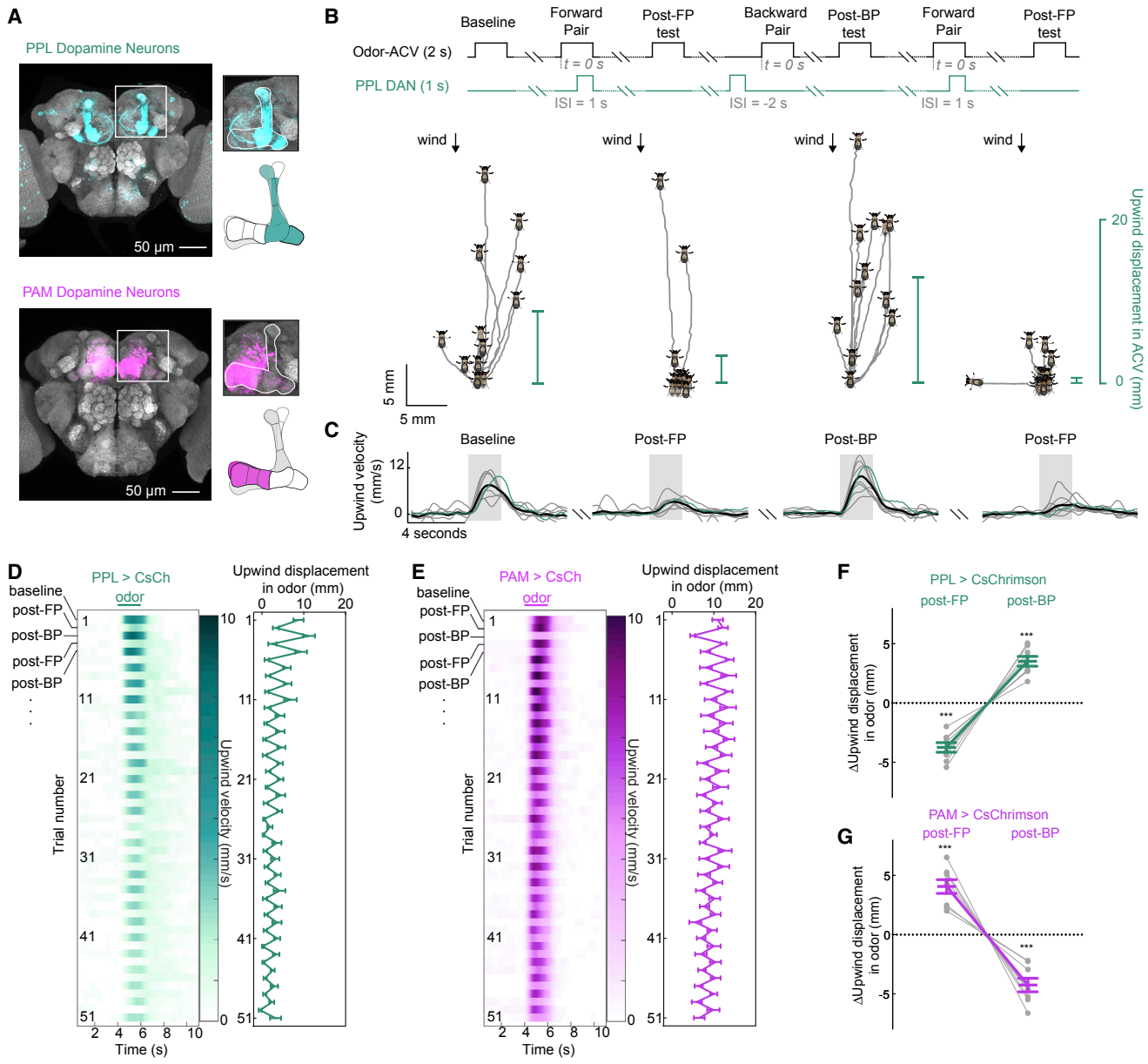

Figure 1. Forward and Backward Conditioning Drives the Formation of Opposing Olfactory Associations

(A) Anatomy of PPL (teal) and PAM (magenta) dopaminergic neuron (DAN) drivers that selectively innervate the mushroom body.

(B) Top: behavioral protocol to compare tracking of apple cider vinegar (ACV) odor after forward pairing (FP) and backward pairing (BP) with optogenetic activation of PPL > CsChrimson flies. Bottom: trajectories of individual flies from a representative experiment, aligned to common origin and wind direction. Flies that did not move in response to the odor were positioned at origin. The odor-evoked upwind displacement of all flies is measured as a change in their center of mass (teal bar).

(C) Upwind velocity of PPL > CsChrimson flies in baseline, post-FP, and post-BP trials (odor indicated by gray box) measured as a change in the center of mass of flies in the upwind direction over the course of a trial. Gray lines: individual experiments; teal line: representative example from (B); black line: mean upwind velocity (n = 8 experiments).

(D) Left: raster plot of mean upwind velocity of PPL > CsChrimson flies across trials. The first row corresponds to the baseline response of naive flies. Subsequent rows show behavioral response to odor after alternating FP and BP trials. Right: mean odor-evoked upwind displacement for the corresponding row in the raster plot.

(E) Same as (D) using PAM > CsChrimson flies.

(F and G) Change in upwind displacement in odor after FP and BP for PPL conditioned (F) and PAM conditioned (G) animals measured relative to the preceding odor trial. n = 8 experiments. One-sample t test against zero with Bonferroni correction: ***$p \leq 0.001$.

For (D)–(G), data are presented as mean ± SEM.

See also Figures S1 and S2 and Video S1.

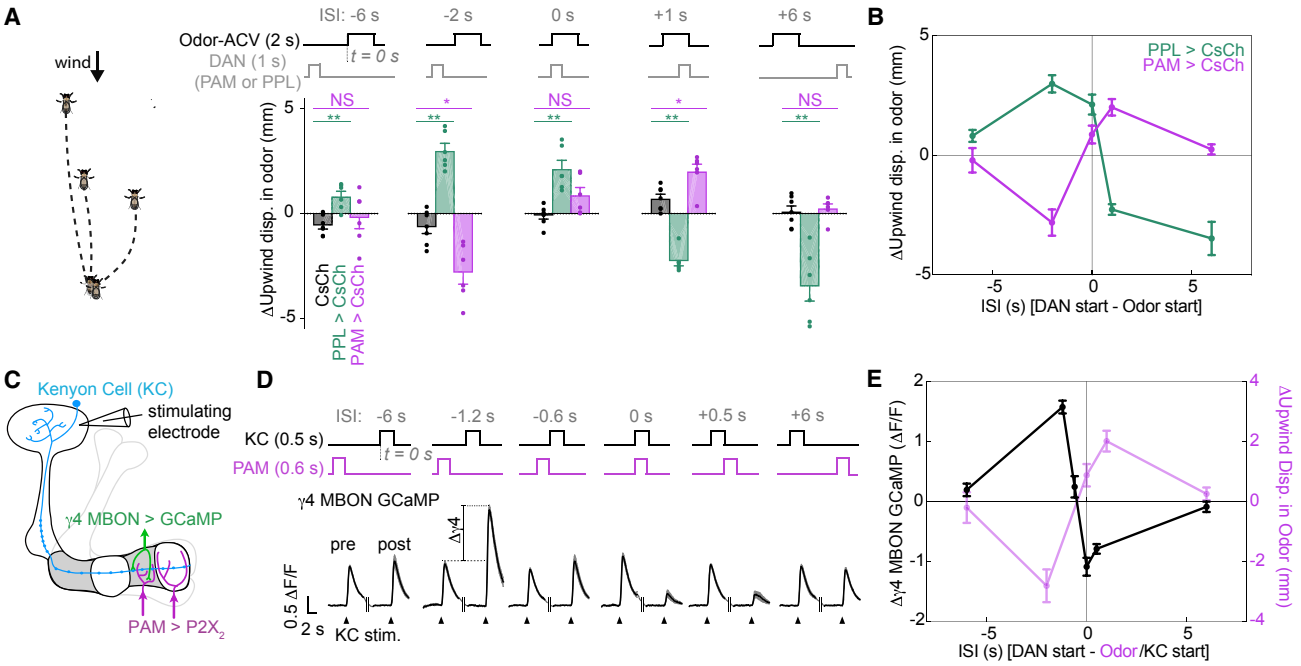

Figure 2. Relating Behavioral and Neural Modulation

(A) Top: protocol varying inter-stimulus interval (ISI) between apple cider vinegar (ACV) odor and optogenetic activation of DANs during behavioral conditioning. Bottom: change in odor-evoked upwind displacement after conditioning, measured relative to the preceding trial. PPL > CsChrimson (teal), PAM > CsChrimson (magenta), and CsChrimson only controls (black). n = 6–7 experiments. Mann-Whitney test with Bonferroni correction: **$p \leq 0.01$, * < 0.05, NS ≥ 0.05.

(B) Overlay of data from (A) to compare temporal dependence of conditioning using PPL and PAM DANs.

(C) Schematic of mushroom body preparation used to measure KC-MBON plasticity.

(D) Top: protocol varying ISI between KC stimulation and chemogenetic activation of DANs during conditioning. Bottom: average KC-evoked responses in the γ4 MBON pre- and post-conditioning with different ISIs. Arrowhead denotes time of KC stimulation.

(E) Black: change in mean peak γ4 MBON response plotted as a function of ISI. n = 5–6 flies for each ISI tested. Magenta: behavioral data for PAM > CsChrimson animals re-plotted from (B). Significant change in γ4 MBON response after pairing was detected for the following ISI: −1.2 s $p \leq 0.001$, 0 s $p < 0.05$, and 0.5 s $p \leq 0.01$; one-sample t test against zero with Bonferroni correction.

All data shown are presented as mean ± SEM.

See also Figure S2.

pairing with either odor exposure or DAN activation alone was insufficient to drive the strong behavioral modulation observed with backward pairing (Figures S1G–S1J). Together, these observations reveal that, during backward pairing, input from both olfactory and dopaminergic pathways is required to rapidly overwrite a prior association and instruct a new odor association of the opposite valence in its place.

Relating Behavioral and Neural Modulation

To examine the temporal sensitivity of associative conditioning, we trained animals for 50 trials while varying the timing between odor and dopaminergic reinforcement, randomly selecting from a set of five different inter-stimulus intervals (ISIs) for each conditioning trial to account for any dependence on the trial structure. Shifting the relative timing between odor presentation and PPL or PAM DAN activation by only a few hundred milliseconds was sufficient to induce a switch from conditioned avoidance to attraction (Figures 2A and 2B), further highlighting that individual flies can dynamically update their associations on a trial-by-trial basis to reflect changes in the predictive value of an odor cue.

What neural mechanism might account for this bidirectional behavioral modulation? One possibility is that distinct compartments within the mushroom body could be sensitive to forward and backward conditioning such that opposing memories are written in parallel at different sites within the circuit, a mechanism proposed for memory extinction (Felsenberg et al., 2018). Alternatively, this bidirectional behavioral modulation could reflect reversible plasticity of KC-MBON synapses within the same compartment. Indeed, dopamine has been shown to bidirectionally tune the strength of KC-MBON signaling, with forward conditioning driving depression of KC-MBON synapses (Cohn et al., 2015; Hige et al., 2015; Owald et al., 2015; Séjourné et al., 2011) while strong dopamine release in the absence of odor leads to synaptic potentiation (Berry et al., 2018; Cohn et al., 2015).

To explore how the timing of dopaminergic input shapes KC-MBON signaling, we initially examined the γ4 compartment whose olfactory signaling undergoes robust dopamine-dependent modulation (Cohn et al., 2015). To gain precise temporal control over both KC and DAN activation, we used a brain explant preparation and directly stimulated KCs by iontophoresing acetylcholine onto their dendrites in the mushroom body

calyx, simulating olfactory input (Figure 2C). Similarly, γ4 DANs were stimulated by expressing the ATP-gated $P2X_2$ channel in the PAM dopaminergic cluster and iontophoresing ATP onto their dendrites. We expressed the genetically encoded calcium indicator GCaMP6s in the γ4 MBON and used KC-evoked dendritic calcium within the γ4 compartment to assess how the strength of KC-MBON signaling was altered following conditioning.

We found that a single forward conditioning trial led to depression of KC-MBON signaling that decayed slowly but could be reversed through a single backward conditioning trial (Figure S3A). Conversely, backward pairing led to lasting synaptic potentiation that could be reversed by a single forward conditioning trial (Figure S3B). Forward and backward pairing therefore bidirectionally regulate KC-MBON signaling on a trial-by-trial basis, mirroring the observed behavioral flexibility (Figures 1B–1G, 2A, and 2B). Varying the timing between KC and DAN stimulation during conditioning revealed a narrow temporal window over which the strength of KC-MBON signaling was bidirectionally modulated, shifting from potentiation when DAN stimulation preceded KC activation to depression when DAN stimulation was concurrent or followed KC activation (Figure 2D). While stronger or more prolonged dopamine release in the absence of an odor has been shown to potentiate KC-MBON signaling (Berry et al., 2018; Cohn et al., 2015), extending the interval between KC and DAN stimulation to 6 s resulted in minimal plasticity (Figure 2D). Importantly, the temporal dependence of KC-MBON plasticity within this compartment matched the timescale of behavioral plasticity evoked using the same PAM dopaminergic reinforcement (Figure 2E), suggesting that bidirectional regulation of KC-MBON signaling may contribute to reversals in behavioral preference.

Bidirectional tuning of KC-MBON synapses appears to represent a shared characteristic of different mushroom body compartments as γ2 and γ5 DANs could also instruct reversible plasticity within their cognate compartments with similar temporal sensitivity (Figures S3C and S3D). Furthermore, comparable synaptic modulation could be driven by DANs when activated by a naturalistic aversive reinforcement, like an electric shock applied to the abdomen of a fly (Figure S3E). Together, these experiments suggest that both PAM and PPL DANs can direct either conditioned avoidance or attraction through bidirectional KC-MBON plasticity in each of the multiple compartments they innervate. This coordinated plasticity can reweight the net output of the mushroom body, biasing animals to avoid odors that predict punishment by depressing the responses of MBONs that mediate approach, including the γ2 MBON (Aso et al., 2014b), to become attracted to odors that predict reward by weakening the responses of MBONs that drive avoidance, like the γ4 or γ5 MBONs (Aso et al., 2014b), or to learn the opposite associations with odors that follow these reinforcements in time by potentiating the activity of these same MBONs.

A Single Reinforcement Can Instruct Multiple Odor Associations

Natural chemical landscapes are often complex such that animals may encounter a variety of odors with different temporal relationships to a reward. Given that odors that precede or follow a reinforcement can be endowed with distinct meaning (Figures 1D–1G), we asked whether animals could rely on differences in the timing of odors relative to a single dopaminergic reinforcement to write multiple olfactory associations in parallel. We trained flies using different pairs of monomolecular odorants with 1 s of PAM neuron activation interposed between them, such that one odor was forward paired while the other was backward paired in time relative to the reinforcement (Figure 3A). We found that a single conditioning trial using this paradigm enhanced upwind tracking to the forward-paired odor while synchronously decreasing tracking of the backward-paired odor. Inverting the order of the two odors in the subsequent conditioning trial had the opposite effect, suppressing attraction to the first odor while enhancing attraction to the second odor (Figures 3B–3D and S4A–S4C). Animals can therefore extract opposing odor associations from the same DAN reinforcement, independent of the identity of the odors used (Figures 3C and S4D).

We replicated this conditioning paradigm in a tethered animal while monitoring the olfactory responses of the γ4 MBON using functional calcium imaging (Figure 3E) and found that a single conditioning trial drove opposing forms of neural plasticity, depressing the response of the γ4 MBON to the forward-paired odor while potentiating the response to the backward-paired odor. As observed behaviorally, inverting the temporal order of the two odors during subsequent conditioning reversed both forms of functional modulation (Figures 3F, S4E, and S4F). Thus, within a compartment, the same dopaminergic signal differentially modulates KC-MBON synapses depending on the relative timing of their activation by different odors, allowing animals to take advantage of the different predictive temporal relationships that exist at any moment in a complex sensory environment.

Directly Relating Neural and Behavioral Plasticity

While our results reveal a striking correspondence between the timescales of neural and behavioral modulation, directly relating these forms of plasticity in *Drosophila* has been difficult in the absence of methods to measure both concurrently. We therefore developed a closed-loop olfactory system, compatible with two-photon imaging, in which a fly's angular velocity on an air-supported ball was yoked to the rotation of a tube carrying a constant airstream. In this assay, a head-fixed animal can control its orientation within the airstream and increase its upwind velocity in response to the introduction of an appetitive olfactory cue, allowing us to image neural activity in the mushroom body during odor-tracking behavior (Figure 4A; Videos S2 and S3). Examining the fictive two-dimensional trajectories of a single animal over multiple odor presentations revealed that forward pairing of ACV with activation of PAM neurons led to increased upwind odor tracking while backward pairing decreased tracking (Figures 4B and S5E). Synchronous imaging of γ4 MBON responses revealed a corresponding functional change: forward pairing depressed the MBON's response to ACV while backward pairing potentiated its response (Figure 4B), consistent with behavioral evidence that γ4 MBON activity contributes to odor avoidance behavior (Aso et al., 2014b). Conditioning reliably evoked bidirectional changes in both odor-evoked upwind displacement and γ4

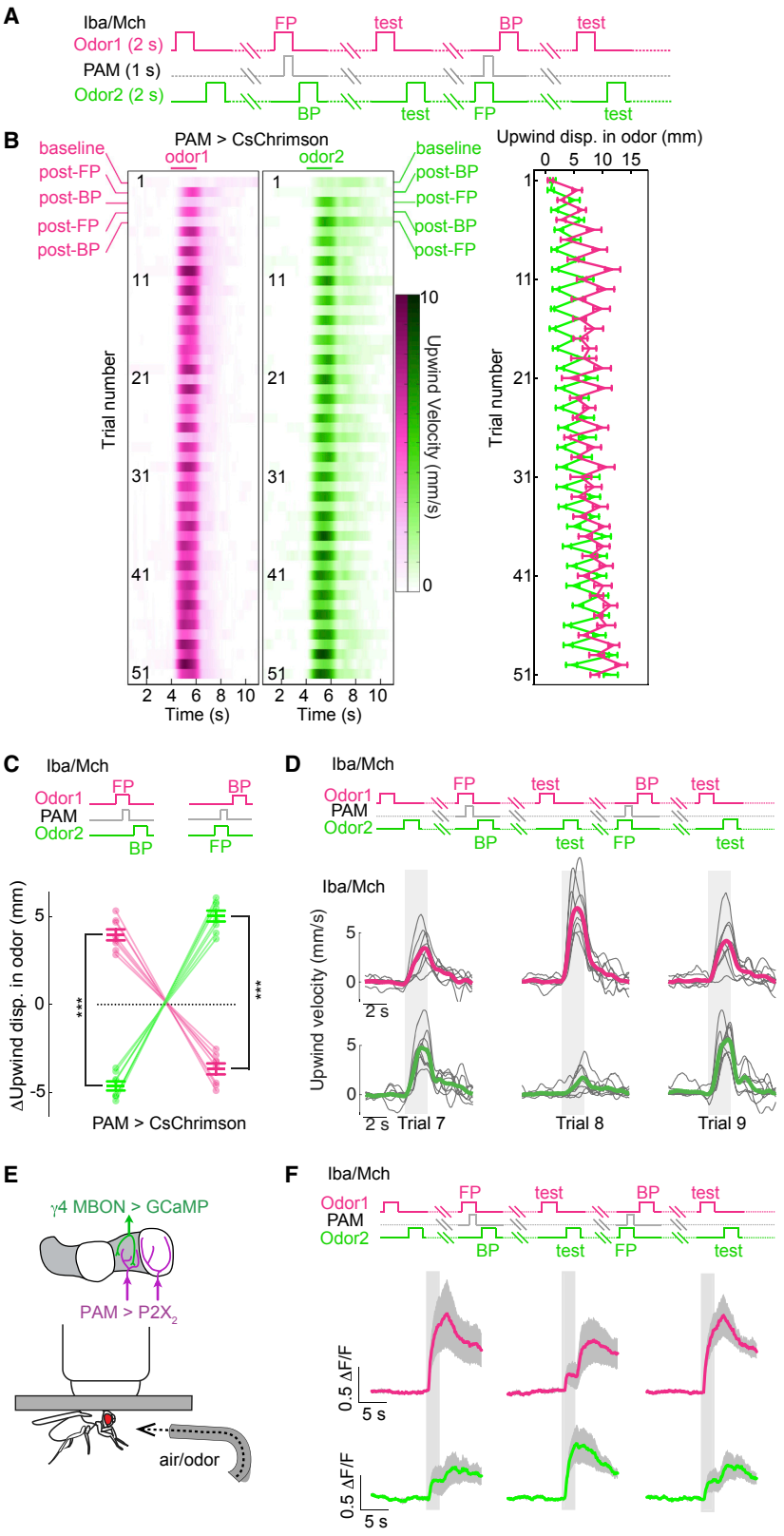

Figure 3. A Single Reinforcement Instructs Multiple Olfactory Associations

(A) Behavioral paradigm to examine how a single dopaminergic reinforcement modulates behavior to two odors that were simultaneously forward paired (FP) or backward paired (BP) with optogenetic activation of PAM > CsChrimson. Odor1, isobutyl acetate (Iba); Odor2, 4-methylcyclohexanol (Mch).

(B) Raster plot of mean upwind velocity of flies for Odor1 (pink) and Odor2 (green). Right: mean odor-evoked upwind displacement for the corresponding rows in the raster plot.

(C) Change in odor-evoked upwind displacement after conditioning, measured relative to the preceding trial.

(D) Upwind velocity of flies during odor presentation using conditioning paradigm shown in (A), trials 7–9 in (B). Time of odor marked by gray box. Gray lines: individual experiments; pink and green lines: average (n = 8 experiments). Paired t test with Bonferroni correction: ***$p \leq 0.001$.

(E) Schematic of *in vivo* preparation to examine modulation of γ4 MBON odor responses.

(F) Top: conditioning paradigm with the same two odors as in (A). Bottom: γ4 MBON responses after conditioning. n = 5 flies.

Data shown in (B), (C), and (F) are mean ± SEM.

See also Figure S4.

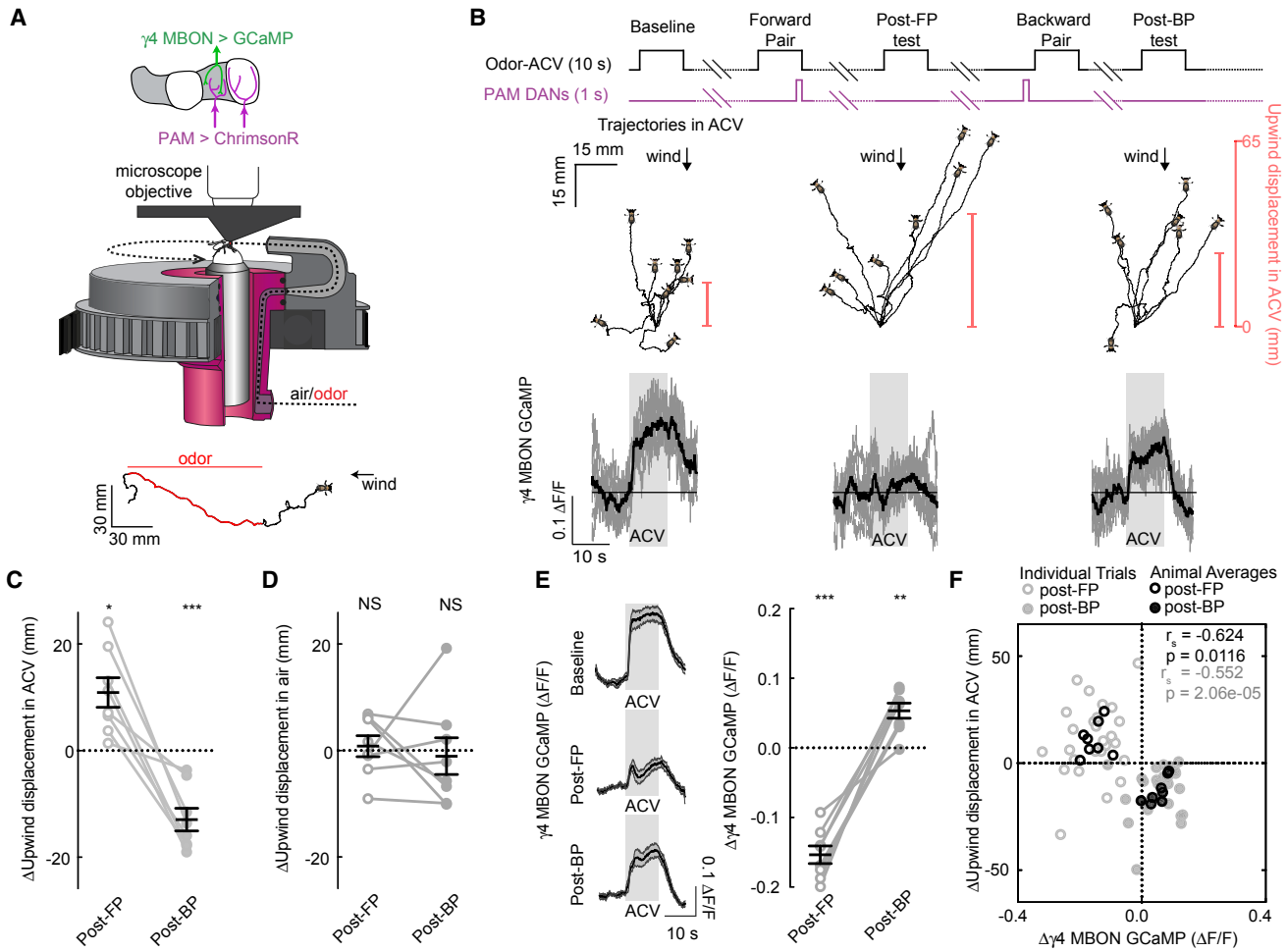

Figure 4. Synchronous Recordings of Neural and Behavioral Plasticity in Individual Flies

(A) Top: strategy to record odor-evoked activity in γ4 MBON and optogenetically activate PAM DANs. Middle: schematic of closed-loop system to synchronously measure MBON activity and odor tracking behavior. Bottom: representative 2D trajectory of a fly presented with apple cider vinegar (ACV) odor (red).

(B) Top: protocol to compare odor-evoked tracking and γ4 MBON responses after forward pairing (post-FP) and backward pairing (post-BP). Middle: fictive 2D trajectories of a single representative fly in baseline, post-FP, and post-BP trials, aligned to a common origin. Average upwind displacement for all trials shown to right (red). Bottom: odor-evoked γ4 MBON responses synchronously recorded in the same animal (odor marked by gray box). Gray lines: odor responses from individual trials; black line: mean odor response for that fly.

(C and D) Mean change in upwind displacement in post-FP and post-BP trials during odor presentation (C) or in clean air (D).

(E) Left: mean γ4 MBON traces for all animals. Right: change in odor-evoked response in γ4 MBON post-FP and post-BP. Data in (C)–(E) represent the mean change in upwind displacement or neural responses measured relative to preceding trial, averaged across 3–4 FP and BP conditioning trials for each animal, n = 8 flies. One-sample t test from zero with Bonferroni correction: ***$p \leq 0.001$, **$p \leq 0.01$, *$p < 0.05$, NS ≥ 0.05.

(F) Change in odor-evoked upwind displacement as a function of change in γ4 MBON responses for individual training trials (gray dots) and animal averages (black dots); n = 27 individual training trials across n = 8 flies; post-FP trials (open circles) and post-BP trials (closed circles).

All data represent mean ± SEM.

See also Figure S5 and Videos S2 and S3.

MBON activity (Figures 4C–4E, S5A–S5D, S5F, and S5G) that were significantly correlated, both on a trial-by-trial basis and across the averaged responses of an individual animal (Figure 4F). Thus, the ability to simultaneously record neural and behavioral plasticity as learning unfolds reveals a tight correspondence between bidirectional changes in KC-MBON signaling within a single compartment and odor attraction. Behavioral modulation, however, likely arises from similar bidirectional plasticity driven synchronously across the multiple mushroom body compartments innervated by the PAM dopaminergic driver (Figure S3C).

Dopamine Receptor Pathways Are Sensitive to Temporal Order

How might the temporal order of olfactory and dopaminergic input be detected within a mushroom body compartment to instruct bidirectional plasticity? One intriguing model is that forward and backward pairing could selectively engage two

dopamine receptors, DopR1 and DopR2 that are co-expressed in the same KCs (Croset et al., 2018) and have been proposed to play opposing roles in the formation and erosion of memories at the behavioral level (Berry et al., 2012; Kim et al., 2007). *In vitro* characterization of these dopamine receptors indicate that they preferentially signal through distinct G-protein partners, with DopR1 coupling to Gαs to stimulate cAMP production (Sugamori et al., 1995) and DopR2 coupling to Gαq to drive increased cytosolic calcium (Feng et al., 1996; Han et al., 1996; Himmelreich et al., 2017).

In vitro, DopR1 and DopR2 exhibit different sensitivities to dopamine (Berry et al., 2012; Himmelreich et al., 2017), raising the possibility that these receptors could be differentially recruited if forward and backward conditioning drove distinct levels of DAN activity and dopamine release. However, monitoring calcium influx in DAN axon terminals revealed that forward and backward conditioning evoked equivalent responses, indistinguishable from direct stimulation of DANs alone (Figures 5A and S6A). Moreover, forward and backward pairing drove comparable levels of dopamine release as measured using either a pHlourin fused to the monoamine transport protein, VMAT (Wu et al., 2013) to visualize pre-synaptic vesicle fusion in DANs (Figures 5B and S6B) or the $GRAB_{DA1m}$ dopamine sensor expressed in post-synaptic KC axons (Sun et al., 2018; Figures 5C and S6C). The $GRAB_{DA1m}$ signal was asymmetrically distributed across the length of KC axons, in accord with dopamine being released in a compartmentalized manner by the activated DANs (Figure S6D). However, the spatial pattern of dopamine release was indistinguishable across conditioning paradigms. Thus, three molecularly distinct sensors suggest that differences in dopaminergic activity cannot account for the opposing forms of neural and behavioral modulation we observe.

Bidirectional plasticity could nevertheless arise from the distinct engagement of DopR1 and DopR2 signaling pathways during forward and backward pairing if either of these receptors or components of their signaling cascades are sensitive to the relative timing of KC and DAN input. We imaged optical reporters of second messengers downstream of Gαs and Gαq during conditioning, focusing on KC axons given that they likely serve as a relevant locus for associative plasticity in the mushroom body (Boto et al., 2014; Cohn et al., 2015; Qin et al., 2012; Zars et al., 2000).

cAMP has been extensively studied as an effector of Gαs signaling that regulates synaptic strength (Kandel et al., 1983; Tomchik and Davis, 2009). We monitored cAMP production (Shafer et al., 2008) in KC axons while varying the relative timing of PAM dopaminergic reinforcement and KC stimulation, using the same ISIs that drove bidirectional plasticity within the γ4 compartment (Figures 2D–2E). cAMP was produced under all conditioning parameters in a spatially compartmentalized manner that mirrored the pattern of dopamine release (Figures 5D, 5E, S6D, and S6E). cAMP was maximally evoked when KC and DAN stimulation were synchronous, matching the timing that gave rise to the strongest depression of KC-MBON signaling (Figures 2E and 5E) and consistent with evidence that calcium-sensitive adenylate cyclases serve as molecular coincidence detectors to amplify cAMP production during associative conditioning (Gervasi et al., 2010; Livingstone et al., 1984; Tomchik and Davis, 2009). However, while forward and backward pairing give rise to opposing forms of neural and behavioral plasticity, these conditioning protocols evoke comparable cAMP production, implying that this second messenger cannot alone encode the temporal order of odor and dopaminergic reinforcement.

We therefore asked whether DopR2 signaling pathways might contribute to the temporal sensitivity of mushroom body plasticity. Upon activation of Gαq, inositol triphosphate (IP_3) is produced, resulting in IP_3-dependent calcium release from the endoplasmic reticulum (ER) (Berridge, 1993). To examine signaling through Gαq, we targeted a low-affinity GCaMP to the ER lumen in KC axons (de Juan-Sanz et al., 2017) and monitored calcium efflux from the ER during conditioning trials. We found that ER calcium in KC axons was selectively released during backward pairing, with no efflux apparent during forward pairing (Figures 5D and 5E). As observed with cAMP production, ER calcium was spatially patterned across the lobe, with greater release evoked in the compartments innervated by the activated DANs (Figure S6F). Application of a Gαq inhibitor blocked ER calcium release during backward pairing (Figure S7C), confirming that it depends on this G-protein pathway. Notably, just as the ISI that evoked maximal cAMP matched the timing of the strongest KC-MBON depression, the ISI that evoked the greatest ER-calcium efflux corresponded to the timing of the strongest potentiation (Figures 2E and 5E). Therefore, while Gαs signaling is sensitive to the temporal coincidence of inputs to the mushroom body during associative conditioning, Gαq signaling depends on their temporal ordering, suggesting that these two pathways may work in concert to generate bidirectional plasticity. Notably, calculating the simple linear difference in the cAMP and ER signals elicited by each pairing protocol replicated the biphasic curve of KC-MBON plasticity (Figure 5F). These observations suggest that, despite potential non-linearities in second-messenger production or signaling through these fluorescent reporters, the selective recruitment of these two second-messenger pathways may account for the temporal dependence of neural and behavioral modulation (Figure 5G).

To confirm that second messenger signaling in KC axons depends on activation of DopR1 and DopR2, we examined cAMP and ER calcium in animals mutant for these dopamine receptors. We first used CRISPR Cas9-mediated genome engineering to generate a novel DopR1 null allele compatible with two-photon imaging (Figures S7A and S7B). In accord with the preferential G-protein signaling of these receptors described *in vitro* (Feng et al., 1996; Han et al., 1996; Himmelreich et al., 2017; Sugamori et al., 1995), production of cAMP was diminished in both forward and backward pairing in DopR1 but not DopR2 mutant flies (Figures 6A and 6B). Conversely, the ER calcium release elicited in backward pairing was lost in DopR2 but not DopR1 mutants (Figures 6C and 6D). In the mushroom body, DopR1 and DopR2 therefore selectively signal through different biochemical cascades to generate distinct patterns of second messengers during conditioning.

DopR1 and DopR2 Underlie Opposing Forms of Plasticity

The temporal sensitivity of DopR1 and DopR2 signaling pathways suggests these receptors play a central role in mediating

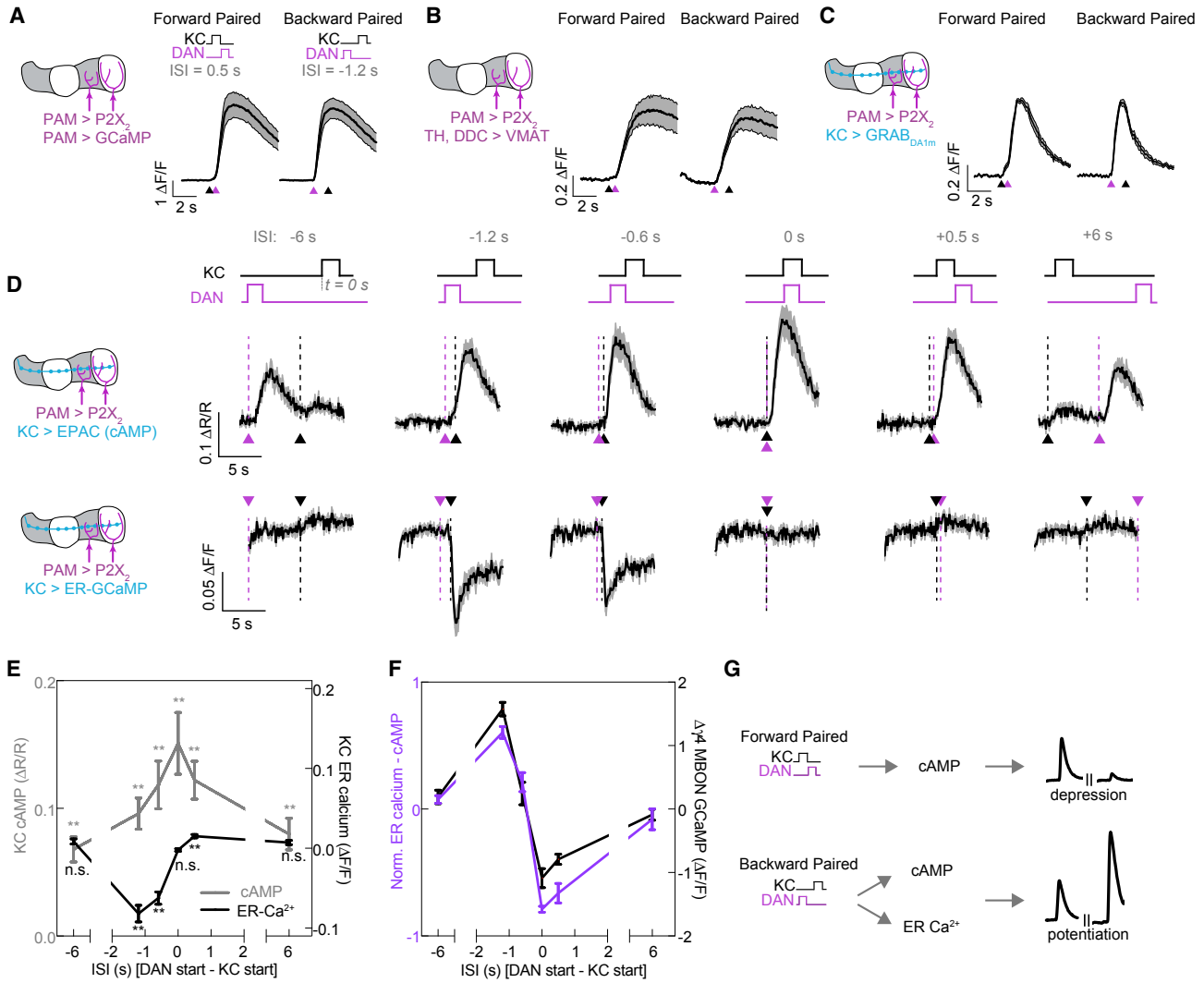

Figure 5. Second-Messenger Pathways are Sensitive to the Order of KC and DAN Input

(A) GCaMP6s responses in the γ4/γ5 DANs during forward (FP) and backward pairing (BP), n = 5 flies.

(B) VMAT-pHluorin signals from γ4/γ5 DANs during FP and BP, n = 5 flies.

(C) Dopamine sensor ($GRAB_{DA1m}$) expressed in KC axons and measured in the γ4/γ5 compartments during FP and BP, n = 7 flies.

(D) cAMP and ER calcium signals in KC axons measured in the γ4/γ5 compartments during conditioning with different ISIs of DAN and KC activation. Top: cAMP production measured as a change in FRET ratio. Bottom: ER calcium efflux. Note that ER-GCaMP fluorecence decreases with release of calcium from ER lumen. Black arrowheads mark time of KC stimulation. Magenta arrowheads mark time of DAN stimulation.

(E) Average cAMP (gray) and ER calcium (black) in γ4/γ5 compartments of KC axons as a function of ISIs tested in (D). n = 6 flies for EPAC; n = 7 flies for ER-GCaMP. One-sample t test against zero with Bonferroni correction: ***p ≤ 0.001, **p ≤ 0.01, *p < 0.05, NS ≥ 0.05.

(F) Left axis (purple): linear difference of normalized cAMP and ER calcium responses from data shown in (E) compared to the timescale of KC-MBON plasticity (right axis, black) (data re-plotted from Figure 2E).

(G) Schematic showing second-messenger production during forward and backward pairing and the resulting plasticity in KC-MBON signaling.

All data represent mean ± SEM.

See also Figure S6.

opposing forms of synaptic plasticity within the mushroom body. Indeed, the robust depression of KC-MBON signaling induced by forward pairing in the γ4 compartment of wild-type animals (Figure 6E) was absent in DopR1 mutants, instead leading to weak potentiation (Figure 6F). By contrast, both forward and backward pairing induced depression of KC-MBON signaling in DopR2 mutants (Figure 6G). Furthermore, inhibition of Gαq prevented potentiation of KC-MBON signaling (Figure S7D), demonstrating that loss of either DopR2 or inhibition of its G-protein partner results in a similar deficit in synaptic plasticity. DopR1 and DopR2 thus play opposing roles in regulating synaptic transmission within the mushroom body, suggesting that the differential signaling through these two receptors underlies the temporally precise bidirectional plasticity we observe.

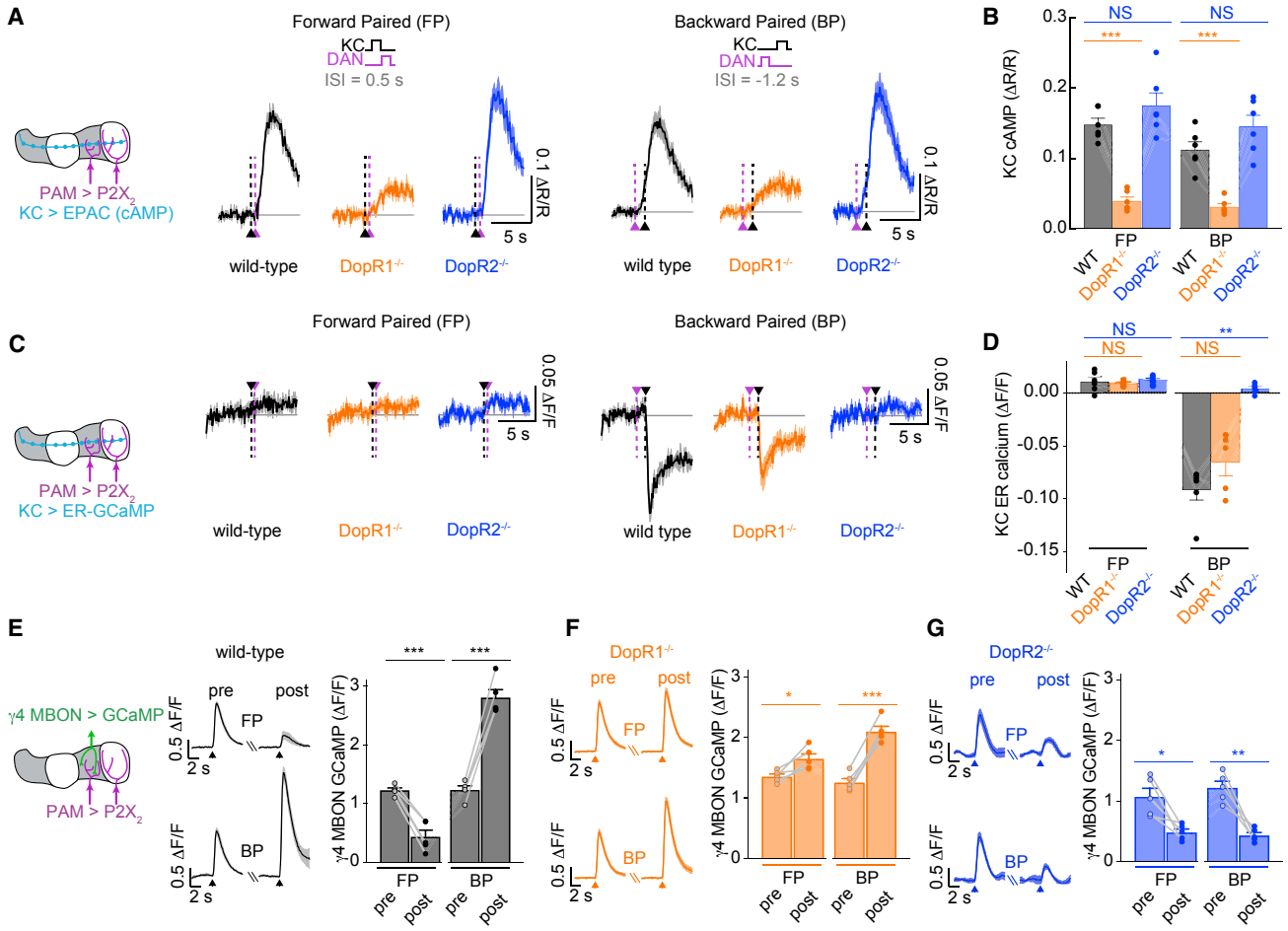

Figure 6. Distinct Roles of DopR1 and DopR2 in Second-Messenger Production and Plasticity

(A–D) cAMP responses (A) and ER calcium responses (C) in KC axons measured in the γ4/γ5 compartments in wild-type (WT), DopR1$^{-/-}$, and DopR2$^{-/-}$ animals during forward (FP) and backward (BP) pairing. Mean cAMP (B) and ER calcium (D) produced in FP and BP. n = 5–6 flies for all genotypes. Unpaired t test with Bonferroni correction (cAMP) or Mann-Whitney test with Bonferroni correction (ER calcium): ***p ≤ 0.001, **p ≤ 0.01, NS ≥ 0.05.

(E) Left: mean γ4 MBON responses to KC stimulation (black arrowhead) pre- and post-FP or pre- and post-BP in wild-type (WT) animals. Right: mean peak response of γ4 MBON to KC stimulation pre- and post-pairing.

(F and G) Same as (E) except in DopR1$^{-/-}$ (F), and DopR2$^{-/-}$ (G) animals. WT data in (E) are re-plotted from ISI = −1.2 s and +0.5 s from Figure 2D. n = 5 flies for all genotypes. Paired t test: ***p ≤ 0.001, **p ≤ 0.01, *p < 0.05.

All data represent mean ± SEM.

See also Figure S7.

At the behavioral level, selective loss of DopR1 or DopR2 rendered animals unable to reversibly update their odor-tracking preferences to reflect the different contingencies of forward and backward conditioning (Figures 7A–7D, S8A, and S8B). While naive odor tracking in DopR1 and DopR2 mutant animals was indistinguishable from wild-type animals (Figures S8E–S8S), DopR1 mutants failed to vigorously track ACV after forward conditioning with PAM activation (Figures 7A, S8A, and S8C), in line with behavioral evidence that DopR1 is required for writing associative memories within the mushroom body (Kim et al., 2007; Qin et al., 2012). Conversely, DopR2 mutant animals strongly tracked ACV following both forward and backward conditioning with PAM activation (Figures 7B, S8B, and S8D); this unwavering attraction suggests that DopR2 mutants are able to form a positive association but unable to overwrite that memory in response to subsequent experience (Berry et al., 2012). The behavioral inflexibility of DopR1 and DopR2 mutants underscores how the balance of signaling through these two receptors allows animals to reversibly modify their behavioral attraction to an odor based on the changing predictive temporal relationships between odor presentation and dopaminergic reinforcement.

DISCUSSION

While memories are often thought of as windows into the past, their adaptive value lies in the ability to predict the future. In this study, we took advantage of the concise circuitry of the *Drosophila* mushroom body to investigate how the precise timing of dopaminergic reinforcement allows animals to form

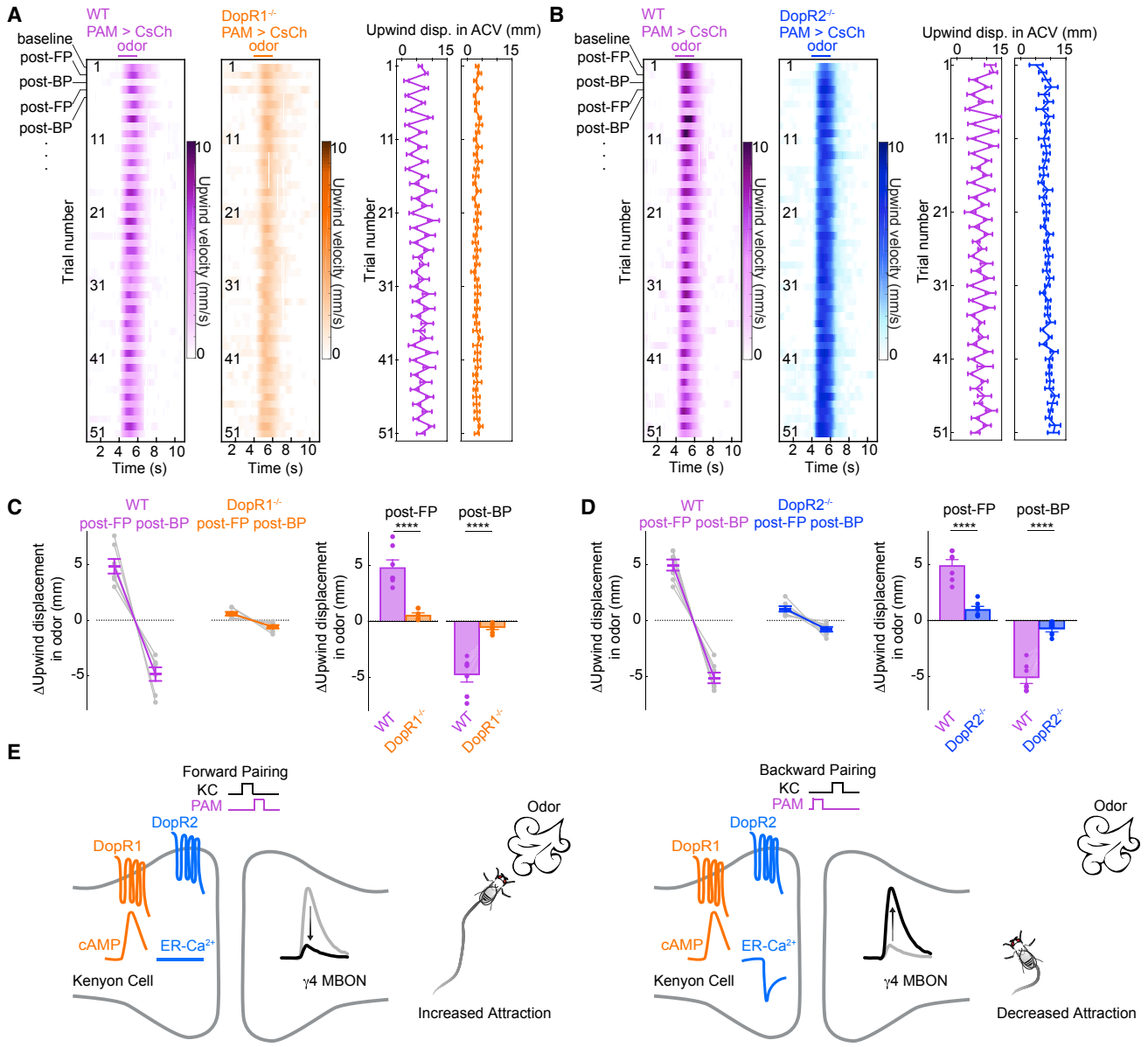

Figure 7. DopR1 and DopR2 Are Required for Behavioral Flexibility

(A) Left: raster plot of average upwind velocity in wild-type (WT, magenta) or DopR1$^{-/-}$ (orange) animals trained by alternating forward pairing (FP) and backward pairing (BP) of PAM > CsChrimson activation with apple cider vinegar (ACV) odor. Right: upwind displacement in odor corresponding to trials shown in raster. Behavioral paradigm is the same as in Figure 1.

(B) Same as (A) except comparing WT (magenta) and DopR2$^{-/-}$ animals (blue).

(C) Change in upwind displacement in odor post-FP and post-BP pairing in WT (magenta) and DopR1$^{-/-}$ (orange) animals measured relative to the preceding odor trial.

(D) Same as (C) except comparing WT and DopR2$^{-/-}$ (blue) animals. n = 7 experiments for all genotypes. Unpaired t test: ****p $\leq$ 0.0001.

(E) Model of how the selective engagement of DopR1 and DopR2 and their downstream signaling pathways during forward and backward conditioning lead to opposing KC-MBON synaptic plasticity and odor-tracking behavior.

All data represent mean ± SEM.

See also Figure S8.

and maintain predictive associations between cues and outcomes. While studies of associative learning have often focused on sensory cues that anticipate punishment or reward, equally informative are cues associated with their termination (Aso and Rubin, 2016; Gerber et al., 2014, 2019; König et al., 2018; Tanimoto et al., 2004). Here, we demonstrate that shifting the relative timing of an odor and reinforcement by <1 s can switch the valence of an olfactory memory, underscoring the exquisite temporal sensitivity of this circuit. As a consequence, flies can form equivalent appetitive associations with odors that anticipate

rewards or follow punishments, or aversive associations with odors that predict punishments or follow rewards. The symmetry of this behavioral modulation permits *Drosophila* to take advantage of all the temporally correlated features of their environment that can be used to infer causal relationships. Together, our work suggests a model in which the steep temporal sensitivity of associative learning arises from the concerted action of two dopamine receptor-signaling pathways that work in opposition to bidirectionally regulate the strength of KC-MBON signaling (Figure 7E), allowing animals to maintain an accurate model of a complex and changing world.

Using Temporal Relationships to Form and Overwrite Associations

In a dynamic environment, memories must be continually retouched and rewritten to maintain their relevance and predictive value. By monitoring how individual flies adapt their odor preferences over 50 conditioning trials, we reveal that *Drosophila* can form and reverse learned associations on a trial-by-trial basis, pointing to the fundamental flexibility of memory updating mechanisms.

Prior work in both *Drosophila* and mammals has suggested memory retention is regulated by multiple mechanisms at different timescales (Bouton, 2002; Davis and Zhong, 2017; Richards and Frankland, 2017). If not reinforced, memories may passively fade over time, reflecting the natural turnover of molecular and neural hardware. Alternatively, memories can be actively eroded either by re-exposure to the learned odor in the absence of the anticipated dopaminergic reinforcement or the reinforcement in the absence of the odor, violating the expected contingency between these two events (Aso and Rubin, 2016; Dunsmoor et al., 2015; Felsenberg et al., 2017). In contrast, the brief episodes of odor and dopaminergic reinforcement (1–2 s) used in our study are insufficient to overwrite an olfactory association when presented independently but can immediately reverse a prior association when paired together in time. The convergence of olfactory and DAN input to the mushroom body thus conveys information about their causal relationship, offering a mechanism to rapidly update memories to reflect the changing temporal structure of the environment.

Mechanisms of Temporal Order Detection

While memory updating could rely on plasticity at various sites within this circuit (Felsenberg et al., 2017, 2018; Shuai et al., 2015), we demonstrate that the bidirectional modulation of behavior is highly correlated with bidirectional changes in the strength of the same KC-MBON synapses within the mushroom body. Such bidirectional synaptic plasticity has been proposed to confer reversibility to learning circuits (Coesmans et al., 2004; Jörntell and Hansel, 2006; Lev-Ram et al., 2002). For example, spike-timing dependent plasticity (STDP) can bidirectionally tune the strength of synaptic connections between neurons depending on the relative timing of spikes in pre- and post-synaptic neurons, mirroring the sensitivity to temporal order observed in associative learning (Bell et al., 1997; Bi and Rubin, 2005; Cassenaer and Laurent, 2012; Dan and Poo, 2004; Drew and Abbott, 2006). However, STDP requires nearly coincident firing patterns on a millisecond timescale, far more rapid than the temporal relationships between stimuli typically required for associative learning. Here, by examining neural and behavioral modulation over the same timescales and even concurrently within the same individuals, we link the modulation of synaptic signaling within the mushroom body to reversible changes in behavior.

Within the mushroom body, each compartment serves as a site of convergence between odor signaling conveyed by KCs and dopaminergic reinforcement, allowing dopamine-receptor pathways within KC axons to detect the temporal order of these inputs. We find that the spatial patterns of dopamine release and dopamine receptor second-messenger cascades adhere to the compartmentalized architecture of the lobes (Boto et al., 2014), permitting different synapses along the same KC axon to be independently regulated (Cohn et al., 2015; Hige et al., 2015). Our observations suggest that within a compartment, multiple neuromodulatory mechanisms tune neurotransmission depending on the temporal structure of conditioning. As a consequence, the distinct complement of KC-MBON synapses activated by odors that precede or follow a reinforcement are differentially regulated, allowing a single dopaminergic reinforcement to drive the synchronous formation of multiple odor associations, effectively enhancing the coding capacity of a compartment.

Dopamine shapes circuit function in diverse ways by engaging distinct classes of receptors that couple to different signaling cascades (Tritsch and Sabatini, 2012). In *Drosophila*, DopR1 and DopR2 have been proposed to play opposing roles in olfactory memory regulation at the behavioral level, with DopR1 essential to memory formation and DopR2 necessary for memory erosion (Berry et al., 2012; Kim et al., 2007; Qin et al., 2012). Yet the contribution of these receptors to synaptic modulation within the mushroom body has remained unclear. Our work reveals that the opposing behavioral roles of DopR1 and DopR2 are mirrored by their antagonistic regulation of KC-MBON signaling, with DopR1 required for the depression ensuing from forward pairing, while DopR2 is essential for the potentiation that follows backward pairing. Although DANs selectively innervating the mushroom body are sufficient to instruct bidirectional behavioral modulation (Aso and Rubin, 2016), the broader expression of DopR1 and DopR2 leaves open the possibility that these receptors may also act at other sites within the nervous system to shape the temporal sensitivity of associative learning.

Using fluorescent sensors of DopR1 and DopR2 second messengers allowed us to gain insight into the spatial and temporal patterning of these intracellular signaling pathways during conditioning. While a potential limitation of optical reporters is their restricted sensitivity and dynamic range, these sensors nevertheless reveal that the selective recruitment of dopamine-receptor signaling cascades is sufficient to account for the temporal dependence of neural and behavioral modulation. Monitoring cAMP production during conditioning reveals that, while the DopR1 pathway serves as a coincidence detector, in accord with the coordinate regulation of adenylate cyclases by Gαs and calcium (Gervasi et al., 2010; Tomchik and Davis, 2009), it cannot autonomously encode the temporal order of events. In contrast, DopR2 signaling through Gαq strictly depends on the temporal sequence of KC and DAN activation.

Which component of the DopR2-signaling cascade is sensitive to the temporal ordering of odor and reinforcement? IP_3 receptors that gate calcium release from the ER lumen represent an intriguing candidate, as their complex regulation by both IP_3 and cytosolic calcium renders them inherently sensitive to the sequence of agonist binding: IP_3 binding unmasks a calcium regulatory site required for channel opening, while high calcium in the absence of IP_3 inhibits channel activity (Adkins and Taylor, 1999; Paknejad and Hite, 2018; Srikanth et al., 2004). Indeed, we observe ER calcium release is time locked to KC stimulation suggesting that the precise order dependence of this pathway relies on calcium entry subsequent to IP_3 production. In the cerebellum, bidirectional plasticity at parallel fiber-Purkinje neuron synapses has been proposed to similarly rely on calcium release from the ER lumen via IP_3 receptors (Finch and Augustine, 1998; Sarkisov and Wang, 2008; Wang et al., 2000). While the analogous circuit organization of the mushroom body and cerebellum has been well described (Farris, 2011), our observations suggest they may share conserved molecular mechanisms for temporally precise synaptic modulation.

The Timescales of Neural Plasticity and Memory

Together, our work points to dopamine receptor signaling pathways in KC axons as a key site of temporal coincidence and order detection during associative learning. While we focused on the role of dopaminergic signaling within the γ4 compartment, we observe that timing-dependent bidirectional plasticity is a shared characteristic of KC-MBON synapses in multiple compartments of the γ lobe. Therefore, the reversible modulation of behavior instructed by both the PAM or PPL DANs likely reflects bidirectional plasticity driven synchronously in the multiple compartments innervated by these DAN drivers. Aversive electric shock and sugar rewards evoke distributed patterns of activity across the DAN population (Burke et al., 2012; Cohn et al., 2015; Liu et al., 2012; Mao and Davis, 2009), implying that these naturalistic reinforcers likewise instruct coordinated bidirectional plasticity across different compartments to rapidly shape the net output of the mushroom body. Similar patterns of DAN activity are also elicited by a fly's locomotion (Berry et al., 2015; Cohn et al., 2015), raising the possibility that, in the context of an odor plume, an animal's behavior may serve as a reinforcement stimulus that itself drives bidirectional synaptic plasticity to regulate odor processing.

The ability to form or overwrite associations on a trial-by-trial basis allows for adaptive behavior in a noisy and uncertain environment where the temporal relationships between events may quickly change. However, animals must also have the capacity to store relevant memories persistently, even for a lifetime. Therefore, the reversible plasticity we observe must co-exist with additional molecular and circuit mechanisms that underlie the formation and retention of longer-term associations. Indeed, recent work has described intrinsic differences between mushroom body compartments in their susceptibility to memory erosion (Aso and Rubin, 2016) as well as differences in second-messenger signaling in distinct KC subpopulations (Boto et al., 2014; Tomchik and Davis, 2009). Together, these results suggest that the differential expression or coupling of dopamine-receptor signaling pathways in different KC classes may tune synaptic plasticity rules to regulate the persistence of information storage. While our work connects molecular pathways within a sub-population of KCs to the emergence of short-term associations, functional dissection of these signaling cascades across the different lobes of the mushroom body will provide insight into the distinct timescales of memory formation and erosion.

STAR★METHODS

Detailed methods are provided in the online version of this paper and include the following:

- KEY RESOURCES TABLE
- LEAD CONTACT AND MATERIALS AVAILABILITY
- EXPERIMENTAL MODEL AND SUBJECT DETAILS
  - Fly strains
- METHOD DETAILS
  - Functional imaging
  - Imaging in *ex vivo* brain explants
  - Behavioral experiments in laminar flow chambers
  - Conditioning with multiple odors in tethered flies
  - Conditioning with electric shock in tethered flies
  - Behavioral and functional imaging in closed-loop system
  - Immunohistochemistry
  - RNA Isolation and qRT-PCR
  - Experimental Design
- QUANTIFICATION AND STATISTICAL ANALYSIS
- DATA AND CODE AVAILABILITY

SUPPLEMENTAL INFORMATION

Supplemental Information can be found online at https://doi.org/10.1016/j.cell.2019.05.040.

ACKNOWLEDGMENTS

We thank Larry Abbott, Barbara Noro, and members of the V.R. lab for valuable discussion and comments on the manuscript. We thank Timothy Ryan, Jaime de Juan-Sanz, Wanhe Li, Gaby Maimon, Jonathan Green, James Petrillo, Patrick Stock, and Josh Salvi for technical advice and Tom Hindmarsh Sten and Nathan Hu for collecting preliminary data. A.H. was supported by NIDCD of the NIH (F31 DC016844) and by the Kavli Neural Systems Institute at The Rockefeller University. V.R. was supported by the New York Stem Cell Foundation, the Pew Foundation, the McKnight Foundation, the Simons Foundation, the Irma T. Hirschl Foundation, the Alfred P. Sloan Foundation, and the NIH (DP2 NS087942).

AUTHOR CONTRIBUTIONS

A.H. performed all experiments and data analysis with input from T.G.W.G., R.C., I.M., and A.S. T.G.W.G. designed and created the fly chamber assay and wrote custom code for data acquisition and analysis. R.C. designed and created the closed-loop system and wrote custom code for data analysis. I.M. generated and characterized the DopR1 mutant. A.S. performed preliminary characterization of dopamine receptor second messenger signaling. J.Z. and Y.L. generated the UAS-GRAB$_{DA}$ flies. A.H. and V.R. wrote the manuscript with input from T.G.W.G., R.C., I.M., and A.S.

DECLARATION OF INTERESTS

The authors declare no competing interests.

Received: August 16, 2018
Revised: February 19, 2019
Accepted: May 20, 2019
Published: June 20, 2019

REFERENCES

Adkins, C.E., and Taylor, C.W. (1999). Lateral inhibition of inositol 1,4,5-trisphosphate receptors by cytosolic Ca(2+). Curr. Biol. *9*, 1115–1118.

Álvarez-Salvado, E., Licata, A.M., Connor, E.G., McHugh, M.K., King, B.M., Stavropoulos, N., Victor, J.D., Crimaldi, J.P., and Nagel, K.I. (2018). Elementary sensory-motor transformations underlying olfactory navigation in walking fruit-flies. eLife *7*, e04577.

Aso, Y., and Rubin, G.M. (2016). Dopaminergic neurons write and update memories with cell-type-specific rules. eLife *5*, 156.

Aso, Y., Siwanowicz, I., Bräcker, L., Ito, K., Kitamoto, T., and Tanimoto, H. (2010). Specific dopaminergic neurons for the formation of labile aversive memory. Curr. Biol. *20*, 1445–1451.

Aso, Y., Herb, A., Ogueta, M., Siwanowicz, I., Templier, T., Friedrich, A.B., Ito, K., Scholz, H., and Tanimoto, H. (2012). Three dopamine pathways induce aversive odor memories with different stability. PLoS Genet. *8*, e1002768.

Aso, Y., Hattori, D., Yu, Y., Johnston, R.M., Iyer, N.A., Ngo, T.T.B., Dionne, H., Abbott, L.F., Axel, R., Tanimoto, H., and Rubin, G.M. (2014a). The neuronal architecture of the mushroom body provides a logic for associative learning. eLife *3*, e04577.

Aso, Y., Sitaraman, D., Ichinose, T., Kaun, K.R., Vogt, K., Belliart-Guérin, G., Plaçais, P.Y., Robie, A.A., Yamagata, N., Schnaitmann, C., et al. (2014b). Mushroom body output neurons encode valence and guide memory-based action selection in *Drosophila*. eLife *3*, e04580.

Bell, J.S., and Wilson, R.I. (2016). Behavior Reveals Selective Summation and Max Pooling among Olfactory Processing Channels. Neuron *91*, 425–438.

Bell, C.C., Han, V.Z., Sugawara, Y., and Grant, K. (1997). Synaptic plasticity in a cerebellum-like structure depends on temporal order. Nature *387*, 278–281.

Berridge, M.J. (1993). Inositol trisphosphate and calcium signalling. Nature *361*, 315–325.

Berry, J.A., Cervantes-Sandoval, I., Nicholas, E.P., and Davis, R.L. (2012). Dopamine is required for learning and forgetting in *Drosophila*. Neuron *74*, 530–542.

Berry, J.A., Cervantes-Sandoval, I., Chakraborty, M., and Davis, R.L. (2015). Sleep Facilitates Memory by Blocking Dopamine Neuron-Mediated Forgetting. Cell *161*, 1656–1667.

Berry, J.A., Phan, A., and Davis, R.L. (2018). Dopamine Neurons Mediate Learning and Forgetting through Bidirectional Modulation of a Memory Trace. Cell Rep. *25*, 651–662.

Bi, G.Q., and Rubin, J. (2005). Timing in synaptic plasticity: from detection to integration. Trends Neurosci. *28*, 222–228.

Boto, T., Louis, T., Jindachomthong, K., Jalink, K., and Tomchik, S.M. (2014). Dopaminergic modulation of cAMP drives nonlinear plasticity across the *Drosophila* mushroom body lobes. Curr. Biol. *24*, 822–831.

Bouton, M.E. (2002). Context, ambiguity, and unlearning: sources of relapse after behavioral extinction. Biol. Psychiatry *52*, 976–986.

Bromberg-Martin, E.S., Matsumoto, M., and Hikosaka, O. (2010). Dopamine in motivational control: rewarding, aversive, and alerting. Neuron *68*, 815–834.

Burke, C.J., Huetteroth, W., Owald, D., Perisse, E., Krashes, M.J., Das, G., Gohl, D., Silies, M., Certel, S., and Waddell, S. (2012). Layered reward signalling through octopamine and dopamine in *Drosophila*. Nature *492*, 433–437.

Campbell, R.A.A., Honegger, K.S., Qin, H., Li, W., Demir, E., and Turner, G.C. (2013). Imaging a population code for odor identity in the *Drosophila* mushroom body. J. Neurosci. *33*, 10568–10581.

Cassenaer, S., and Laurent, G. (2012). Conditional modulation of spike-timing-dependent plasticity for olfactory learning. Nature *482*, 47–52.

Claridge-Chang, A., Roorda, R.D., Vrontou, E., Sjulson, L., Li, H., Hirsh, J., and Miesenböck, G. (2009). Writing memories with light-addressable reinforcement circuitry. Cell *139*, 405–415.

Coesmans, M., Weber, J.T., De Zeeuw, C.I., and Hansel, C. (2004). Bidirectional parallel fiber plasticity in the cerebellum under climbing fiber control. Neuron *44*, 691–700.

Cohn, R., Morantte, I., and Ruta, V. (2015). Coordinated and Compartmentalized Neuromodulation Shapes Sensory Processing in *Drosophila*. Cell *163*, 1742–1755.

Connolly, J.B., Roberts, I.J., Armstrong, J.D., Kaiser, K., Forte, M., Tully, T., and O'Kane, C.J. (1996). Associative learning disrupted by impaired Gs signaling in *Drosophila* mushroom bodies. Science *274*, 2104–2107.

Croset, V., Treiber, C.D., and Waddell, S. (2018). Cellular diversity in the *Drosophila* midbrain revealed by single-cell transcriptomics. eLife *7*, 312.

Dan, Y., and Poo, M.M. (2004). Spike timing-dependent plasticity of neural circuits. Neuron *44*, 23–30.

Davis, R.L., and Zhong, Y. (2017). The Biology of Forgetting-A Perspective. Neuron *95*, 490–503.

de Juan-Sanz, J., Holt, G.T., Schreiter, E.R., de Juan, F., Kim, D.S., and Ryan, T.A. (2017). Axonal Endoplasmic Reticulum Ca^{2+} Content Controls Release Probability in CNS Nerve Terminals. Neuron *93*, 867–881.

Drew, P.J., and Abbott, L.F. (2006). Extending the effects of spike-timing-dependent plasticity to behavioral timescales. Proc. Natl. Acad. Sci. USA *103*, 8876–8881.

Dunsmoor, J.E., Niv, Y., Daw, N., and Phelps, E.A. (2015). Rethinking Extinction. Neuron *88*, 47–63.

Farris, S.M. (2011). Are mushroom bodies cerebellum-like structures? Arthropod Struct. Dev. *40*, 368–379.

Felsenberg, J., Barnstedt, O., Cognigni, P., Lin, S., and Waddell, S. (2017). Re-evaluation of learned information in *Drosophila*. Nature *544*, 240–244.

Felsenberg, J., Jacob, P.F., Walker, T., Barnstedt, O., Edmondson-Stait, A.J., Pleijzier, M.W., Otto, N., Schlegel, P., Sharifi, N., Perisse, E., et al. (2018). Integration of Parallel Opposing Memories Underlies Memory Extinction. Cell *175*, 709–722.

Feng, G., Hannan, F., Reale, V., Hon, Y.Y., Kousky, C.T., Evans, P.D., and Hall, L.M. (1996). Cloning and functional characterization of a novel dopamine receptor from *Drosophila* melanogaster. J. Neurosci. *16*, 3925–3933.

Finch, E.A., and Augustine, G.J. (1998). Local calcium signalling by inositol-1,4,5-trisphosphate in Purkinje cell dendrites. Nature *396*, 753–756.

Friggi-Grelin, F., Coulom, H., Meller, M., Gomez, D., Hirsh, J., and Birman, S. (2003). Targeted gene expression in *Drosophila* dopaminergic cells using regulatory sequences from tyrosine hydroxylase. J. Neurobiol. *54*, 618–627.

Ge, D.T., Tipping, C., Brodsky, M.H., and Zamore, P.D. (2016). Rapid Screening for CRISPR-Directed Editing of the *Drosophila* Genome Using white Coconversion. G3 (Bethesda) *6*, 3197–3206.

Gerber, B., Yarali, A., Diegelmann, S., Wotjak, C.T., Pauli, P., and Fendt, M. (2014). Pain-relief learning in flies, rats, and man: basic research and applied perspectives. Learn. Mem. *21*, 232–252.

Gerber, B., König, C., Fendt, M., Andreatta, M., Romanos, M., Pauli, P., and Yarali, A. (2019). Timing-dependent valence reversal: a principle of reinforcement processing and its possible implications. Curr. Opin. Behav. Sci. *26*, 114–120.

Gervasi, N., Tchénio, P., and Preat, T. (2010). PKA dynamics in a *Drosophila* learning center: coincidence detection by rutabaga adenylyl cyclase and spatial regulation by dunce phosphodiesterase. Neuron *65*, 516–529.

Green, J., Adachi, A., Shah, K.K., Hirokawa, J.D., Magani, P.S., and Maimon, G. (2017). A neural circuit architecture for angular integration in *Drosophila*. Nature *546*, 101–106.

Han, K.A., Millar, N.S., Grotewiel, M.S., and Davis, R.L. (1996). DAMB, a novel dopamine receptor expressed specifically in *Drosophila* mushroom bodies. Neuron *16*, 1127–1135.

Heisenberg, M. (2003). Mushroom body memoir: from maps to models. Nat. Rev. Neurosci. *4*, 266–275.

Hige, T. (2018). What can tiny mushrooms in fruit flies tell us about learning and memory? Neurosci. Res. *129*, 8–16.

Hige, T., Aso, Y., Modi, M.N., Rubin, G.M., and Turner, G.C. (2015). Heterosynaptic Plasticity Underlies Aversive Olfactory Learning in *Drosophila*. Neuron *88*, 985–998.

Himmelreich, S., Masuho, I., Berry, J.A., MacMullen, C., Skamangas, N.K., Martemyanov, K.A., and Davis, R.L. (2017). Dopamine Receptor DAMB Signals via Gq to Mediate Forgetting in *Drosophila*. Cell Rep. *21*, 2074–2081.

Jenett, A., Rubin, G.M., Ngo, T.T.B., Shepherd, D., Murphy, C., Dionne, H., Pfeiffer, B.D., Cavallaro, A., Hall, D., Jeter, J., et al. (2012). A GAL4-driver line resource for *Drosophila* neurobiology. Cell Rep. *2*, 991–1001.

Jörntell, H., and Hansel, C. (2006). Synaptic memories upside down: bidirectional plasticity at cerebellar parallel fiber-Purkinje cell synapses. Neuron *52*, 227–238.

Kandel, E.R., Abrams, T., Bernier, L., Carew, T.J., Hawkins, R.D., and Schwartz, J.H. (1983). Classical conditioning and sensitization share aspects of the same molecular cascade in Aplysia. Cold Spring Harb. Symp. Quant. Biol. *48*, 821–830.

Keleman, K., Vrontou, E., Krüttner, S., Yu, J.Y., Kurtovic-Kozaric, A., and Dickson, B.J. (2012). Dopamine neurons modulate pheromone responses in *Drosophila* courtship learning. Nature *489*, 145–149.

Kim, Y.C., Lee, H.G., and Han, K.A. (2007). D1 dopamine receptor dDA1 is required in the mushroom body neurons for aversive and appetitive learning in *Drosophila*. J. Neurosci. *27*, 7640–7647.

König, C., Khalili, A., Ganesan, M., Nishu, A.P., Garza, A.P., Niewalda, T., Gerber, B., Aso, Y., and Yarali, A. (2018). Reinforcement signaling of punishment versus relief in fruit flies. Learn. Mem. *25*, 247–257.

Lebestky, T., Chang, J.S.C., Dankert, H., Zelnik, L., Kim, Y.C., Han, K.A., Wolf, F.W., Perona, P., and Anderson, D.J. (2009). Two different forms of arousal in *Drosophila* are oppositely regulated by the dopamine D1 receptor ortholog DopR via distinct neural circuits. Neuron *64*, 522–536.

Lerner, T.N., Shilyansky, C., Davidson, T.J., Evans, K.E., Beier, K.T., Zalocusky, K.A., Crow, A.K., Malenka, R.C., Luo, L., Tomer, R., and Deisseroth, K. (2015). Intact-Brain Analyses Reveal Distinct Information Carried by SNc Dopamine Subcircuits. Cell *162*, 635–647.

Lev-Ram, V., Wong, S.T., Storm, D.R., and Tsien, R.Y. (2002). A new form of cerebellar long-term potentiation is postsynaptic and depends on nitric oxide but not cAMP. Proc. Natl. Acad. Sci. USA *99*, 8389–8393.

Li, H., Chaney, S., Roberts, I.J., Forte, M., and Hirsh, J. (2000). Ectopic G-protein expression in dopamine and serotonin neurons blocks cocaine sensitization in *Drosophila melanogaster*. Curr. Biol. *10*, 211–214.

Liu, C., Plaçais, P.Y., Yamagata, N., Pfeiffer, B.D., Aso, Y., Friedrich, A.B., Siwanowicz, I., Rubin, G.M., Preat, T., and Tanimoto, H. (2012). A subset of dopamine neurons signals reward for odour memory in *Drosophila*. Nature *488*, 512–516.

Livingstone, M.S., Sziber, P.P., and Quinn, W.G. (1984). Loss of calcium/calmodulin responsiveness in adenylate cyclase of rutabaga, a *Drosophila* learning mutant. Cell *37*, 205–215.

Mao, Z., and Davis, R.L. (2009). Eight different types of dopaminergic neurons innervate the *Drosophila* mushroom body neuropil: anatomical and physiological heterogeneity. Front. Neural Circuits *3*, 5.

Mauk, M.D., and Donegan, N.H. (1997). A model of Pavlovian eyelid conditioning based on the synaptic organization of the cerebellum. Learn. Mem. *4*, 130–158.

Moore, R.J.D., Taylor, G.J., Paulk, A.C., Pearson, T., van Swinderen, B., and Srinivasan, M.V. (2014). FicTrac: a visual method for tracking spherical motion and generating fictive animal paths. J. Neurosci. Methods *225*, 106–119.

Owald, D., and Waddell, S. (2015). Olfactory learning skews mushroom body output pathways to steer behavioral choice in *Drosophila*. Curr. Opin. Neurobiol. *35*, 178–184.

Owald, D., Felsenberg, J., Talbot, C.B., Das, G., Perisse, E., Huetteroth, W., and Waddell, S. (2015). Activity of defined mushroom body output neurons underlies learned olfactory behavior in *Drosophila*. Neuron *86*, 417–427.

Paknejad, N., and Hite, R.K. (2018). Structural basis for the regulation of inositol trisphosphate receptors by Ca^{2+} and IP_3. Nat. Struct. Mol. Biol. *25*, 660–668.

Pavlov, P.I. (1927). Conditioned Reflexes: An Investigation of the Physiological Activity of the Cerebral Cortex (Oxford University Press).

Pfeiffer, B.D., Ngo, T.T.B., Hibbard, K.L., Murphy, C., Jenett, A., Truman, J.W., and Rubin, G.M. (2010). Refinement of tools for targeted gene expression in *Drosophila*. Genetics *186*, 735–755.

Pfeiffer, B.D., Truman, J.W., and Rubin, G.M. (2012). Using translational enhancers to increase transgene expression in *Drosophila*. Proc. Natl. Acad. Sci. USA *109*, 6626–6631.

Pignatelli, M., and Bonci, A. (2015). Role of Dopamine Neurons in Reward and Aversion: A Synaptic Plasticity Perspective. Neuron *86*, 1145–1157.

Qin, H., Cressy, M., Li, W., Coravos, J.S., Izzi, S.A., and Dubnau, J. (2012). Gamma neurons mediate dopaminergic input during aversive olfactory memory formation in *Drosophila*. Curr. Biol. *22*, 608–614.

Rescorla, R.A. (1988). Behavioral studies of Pavlovian conditioning. Annu. Rev. Neurosci. *11*, 329–352.

Richards, B.A., and Frankland, P.W. (2017). The Persistence and Transience of Memory. Neuron *94*, 1071–1084.

Sarkisov, D.V., and Wang, S.S.H. (2008). Order-dependent coincidence detection in cerebellar Purkinje neurons at the inositol trisphosphate receptor. J. Neurosci. *28*, 133–142.

Schultz, W., Dayan, P., and Montague, P.R. (1997). A neural substrate of prediction and reward. Science *275*, 1593–1599.

Seelig, J.D., and Jayaraman, V. (2015). Neural dynamics for landmark orientation and angular path integration. Nature *521*, 186–191.

Séjourné, J., Plaçais, P.Y., Aso, Y., Siwanowicz, I., Trannoy, S., Thoma, V., Tedjakumala, S.R., Rubin, G.M., Tchénio, P., Ito, K., et al. (2011). Mushroom body efferent neurons responsible for aversive olfactory memory retrieval in *Drosophila*. Nat. Neurosci. *14*, 903–910.

Shafer, O.T., Kim, D.J., Dunbar-Yaffe, R., Nikolaev, V.O., Lohse, M.J., and Taghert, P.H. (2008). Widespread receptivity to neuropeptide PDF throughout the neuronal circadian clock network of *Drosophila* revealed by real-time cyclic AMP imaging. Neuron *58*, 223–237.

Shuai, Y., Hirokawa, A., Ai, Y., Zhang, M., Li, W., and Zhong, Y. (2015). Dissecting neural pathways for forgetting in *Drosophila* olfactory aversive memory. Proc. Natl. Acad. Sci. USA *112*, E6663–E6672.

Srikanth, S., Wang, Z., Tu, H., Nair, S., Mathew, M.K., Hasan, G., and Bezprozvanny, I. (2004). Functional properties of the *Drosophila melanogaster* inositol 1,4,5-trisphosphate receptor mutants. Biophys. J. *86*, 3634–3646.

Steck, K., Veit, D., Grandy, R., Badia, S.B.I., Badia, S.B.I., Mathews, Z., Verschure, P., Hansson, B.S., and Knaden, M. (2012). A high-throughput behavioral paradigm for *Drosophila* olfaction - The Flywalk. Sci. Rep. *2*, 361.

Sugamori, K.S., Demchyshyn, L.L., McConkey, F., Forte, M.A., and Niznik, H.B. (1995). A primordial dopamine D1-like adenylyl cyclase-linked receptor from *Drosophila melanogaster* displaying poor affinity for benzazepines. FEBS Lett. *362*, 131–138.

Sun, F., Zeng, J., Jing, M., Zhou, J., Feng, J., Owen, S.F., Luo, Y., Li, F., Wang, H., Yamaguchi, T., et al. (2018). A Genetically Encoded Fluorescent Sensor Enables Rapid and Specific Detection of Dopamine in Flies, Fish, and Mice. Cell *174*, 481–496.

Surmeier, D.J., Plotkin, J., and Shen, W. (2009). Dopamine and synaptic plasticity in dorsal striatal circuits controlling action selection. Curr. Opin. Neurobiol. *19*, 621–628.

Tanaka, N.K., Tanimoto, H., and Ito, K. (2008). Neuronal assemblies of the *Drosophila* mushroom body. J. Comp. Neurol. *508*, 711–755.

Tanimoto, H., Heisenberg, M., and Gerber, B. (2004). Experimental psychology: event timing turns punishment to reward. Nature *430*, 983–983.

Tomchik, S.M., and Davis, R.L. (2009). Dynamics of learning-related cAMP signaling and stimulus integration in the *Drosophila* olfactory pathway. Neuron *64*, 510–521.

Tritsch, N.X., and Sabatini, B.L. (2012). Dopaminergic modulation of synaptic transmission in cortex and striatum. Neuron *76*, 33–50.

Tully, T., and Quinn, W.G. (1985). Classical conditioning and retention in normal and mutant *Drosophila melanogaster*. J. Comp. Physiol. A Neuroethol. Sens. Neural Behav. Physiol. *157*, 263–277.

Turner, G.C., Bazhenov, M., and Laurent, G. (2008). Olfactory representations by *Drosophila* mushroom body neurons. J. Neurophysiol. *99*, 734–746.

Waddell, S. (2016). Neural Plasticity: Dopamine Tunes the Mushroom Body Output Network. Curr. Biol. *26*, R109–R112.

Wang, S.S., Denk, W., and Häusser, M. (2000). Coincidence detection in single dendritic spines mediated by calcium release. Nat. Neurosci. *3*, 1266–1273.

Wu, T.H., Lu, Y.N., Chuang, C.L., Wu, C.L., Chiang, A.S., Krantz, D.E., and Chang, H.Y. (2013). Loss of vesicular dopamine release precedes tauopathy in degenerative dopaminergic neurons in a *Drosophila* model expressing human tau. Acta Neuropathol. *125*, 711–725.

Yamagata, N., Ichinose, T., Aso, Y., Plaçais, P.Y., Friedrich, A.B., Sima, R.J., Preat, T., Rubin, G.M., and Tanimoto, H. (2015). Distinct dopamine neurons mediate reward signals for short- and long-term memories. Proc. Natl. Acad. Sci. USA *112*, 578–583.

Yao, Z., Macara, A.M., Lelito, K.R., Minosyan, T.Y., and Shafer, O.T. (2012). Analysis of functional neuronal connectivity in the *Drosophila* brain. J. Neurophysiol. *108*, 684–696.

Zars, T., Wolf, R., Davis, R., and Heisenberg, M. (2000). Tissue-specific expression of a type I adenylyl cyclase rescues the rutabaga mutant memory defect: in search of the engram. Learn. Mem. *7*, 18–31.

STAR★METHODS

KEY RESOURCES TABLE

REAGENT or RESOURCE	SOURCE	IDENTIFIER
Antibodies		
anti-DAMB	Ronald Davis (Feng et al., 1996)	N/A
anti-DopR	Tim Lebetsky (Lebestky et al., 2009)	N/A
anti-GFP	Abcam	ab13970; RRID:AB_300798
anti-brp	Developmental Studies Hybridoma Bank	nc82; RRID:AB_2314866
Chemicals, Peptides, and Recombinant Proteins		
All trans-Retinal	Sigma-Aldrich	R2500
Collagenase	Sigma-Aldrich	C0130
Acetylcholine chloride	Sigma-Aldrich	A2661
ATP, disodium salt hydrate	Sigma-Aldrich	A2383
YM-254890	Wako Chemicals	257-00631
Apple Cider Vinegar	Heinz	N/A
Benzaldehyde	Sigma-Aldrich	418099
1-Hexanol	Sigma-Aldrich	H13303
Isobutyl Acetate	Sigma-Aldrich	537570
Mineral Oil, Heavy	Fisher Chemical	O122-4
Experimental Models: Organisms/Strains		
Drosophila: 20X-UAS-CsChrimson.mVenus-attP18	Vivek Jayaraman, Janelia Research Campus	BDSC_55134
Drosophila: 20X-UAS-CsChrimson.mVenus-attP40	Vivek Jayaraman, Janelia Research Campus	BDSC_55135
Drosophila: 20X-UAS-ChrimsonR.mCherry-attP2	Vivek Jayaraman, Janelia Research Campus	N/A
Drosophila: VT026001-Gal4	Vienna *Drosophila* Resource Center	VDRC: 202414
Drosophila: MB042B	Bloomington *Drosophila* Stock Center; (Aso et al., 2014a)	BDSC_68303
Drosophila: MB504B	Bloomington *Drosophila* Stock Center; (Aso et al., 2014a)	BDSC_68329
Drosophila: R53C03-LexA	Bloomington *Drosophila* Stock Center; (Pfeiffer et al., 2010)	BDSC_52861
Drosophila: R58E02-LexA	Bloomington *Drosophila* Stock Center; (Pfeiffer et al., 2010)	BDSC_52740
Drosophila: UAS-GCaMP6s	Bloomington *Drosophila* Stock Center	BDSC_42749; BDSC_42746
Drosophila: LexAOP-GCaMP6s	Bloomington *Drosophila* Stock Center	BDSC_ 44589
Drosophila: OK107-Gal4	(Connolly et al., 1996)	N/A
Drosophila: TH-Gal4	(Friggi-Grelin et al., 2003)	N/A
Drosophila: DDC-Gal4	(Li et al., 2000)	N/A
Drosophila: LexAOP-P2X$_2$	Orie Shafer; (Yao et al., 2012)	N/A
Drosophila: UAS-EPAC	(Shafer et al., 2008)	N/A
Drosophila: DopR2$^{attP/attP}$ (DopR2$^{-/-}$)	(Keleman et al., 2012)	N/A
Drosophila: UAS-GRAB$_{DA1m}$	(Sun et al., 2018)	BDSC_80048
Drosophila: UAS-VMAT-pHluorin	(Wu et al., 2013)	N/A
Drosophila: 66C08-Gal4	Bloomington *Drosophila* Stock Center; (Jenett et al., 2012)	BDSC_49412
Drosophila: 73F07-LexA	Bloomington *Drosophila* Stock Center; (Pfeiffer et al., 2010)	BDSC_52743
Drosophila: 25D01-Gal4	Bloomington *Drosophila* Stock Center; (Jenett et al., 2012)	BDSC_49122

(*Continued on next page*)

Continued

REAGENT or RESOURCE	SOURCE	IDENTIFIER
Drosophila: 25D01-LexA	Bloomington *Drosophila* Stock Center; (Pfeiffer et al., 2010)	BDSC_53519
Drosophila: nos-Cas	Bloomington *Drosophila* Stock Center	BDSC_54591
Oligonucleotides		
DopR1 gRNA1: ATG AAT GGA TGG TTG GTG GA	This paper	N/A
DopR1 gRNA2: GAG ACG GAG CTG CTG TAG GC	This paper	N/A
DopR1 gRNA1 pCFD4: TAT ATA GGA AAG ATA TCC GGG TGA ACT TCG ATG AAT GGA TGG TTG GTG GAG TTT TAG AGC TAG AAA TAG CAA G	This paper	N/A
DopR1 gRNA2 PCFD4: ATT TTA ACT TGC TAT TTC TAG CTC TAA AAC GCC TAC AGC AGC TCC GTC TCG ACG TTA AAT TGA AAA TAG GTC	This paper	N/A
UAS-ER-GCaMP210: GCG GCT CGA GGG TAC CAA CTT AAA AAA AAA AAT CAA ACA AAA TGG GAC TGC TGT CTG TGC CTC	This paper	N/A
UAS-ER-GCaMP210: TTC ATT CTA GAT CAC AGC TCA TCC TTG CCT CCG	This paper	N/A
Recombinant DNA		
pJFRC81	Addgene Plasmid; (Pfeiffer et al., 2012)	36432
ER-GCaMP6-210	Timothy Ryan; (de Juan-Sanz et al., 2017)	N/A
pCFD4	Addgene Plasmid; (Ge et al., 2016)	83954
Software and Algorithms		
GraphPad Prism 7	GraphPad Software	https://www.graphpad.com/scientific-software/prism/
Python	Python Software Foundation	https://www.python.org/
FicTrac	(Moore et al., 2014)	http://rjdmoore.net/fictrac/
MATLAB	MathWorks	https://www.mathworks.com/
Adobe Illustrator CC	Adobe Systems	https://www.adobe.com/products/illustrator.html
Fiji	NIH	http://fiji.sc/
Other		
A4988 Stepper Motor Driver Carrier	Pololu	2980
Bipolar Stepper Motor	Pololu	1206
Dust-Free Timing Belt XL Series, 1/4" width	McMaster-Carr	1679K121
Ultra-Corrosion-Resistant Stainless Steel Ball Bearing	McMaster-Carr	5908K19
Oil Resistant O-Rings	McMaster-Carr	2418T126
565 nm LED Microscope Light	CoolLED	PE-100
Red (627nm) LUXEON Rebel LED	Luxeon	SR-05-D2050
Heat Sinks 35X35X10mm ADHV MNT	Mouser	532-374624B32G
Scratch-Resistant Acrylic	McMaster-Carr	8505K754
Recom Power RCD-24-0.70/W/X2	Digikey	945-1617-ND
DC12V SMD3528-300-IR InfraRed (850nm/940nm) Single Chip Flexible LED Strips 60LEDs 4.8W Per Meter	LED Lights World	N/A
Z ZTDM Lab Home DC Power Supply Tool 30V 0-5A US 110V QW-MS305D	Amazon	N/A
KNACRO DC-DC 12V to 3.3V 2A Step-down power supply module	Amazon	N/A
VO14642AT solid state relay	Mouser Electronics	782-VO14642AT
12V DC 2-position 3-way Micro Mini Electric Solenoid Valve for Gas Air/Pump	eBay	N/A

(*Continued on next page*)

Continued

REAGENT or RESOURCE	SOURCE	IDENTIFIER
1.5 mm-Thick Clear Acrylic (Clear Cast Acrylic Sheet, 12" x 24" x 1/16")	McMaster-Carr	8560K172
3 mm-Thick Black Acrylic (Black Scratch-Resistant Acrylic, 12" x 24" x 1/8")	McMaster-Carr	8505K742
Cole-Parmer Female Luer x 10-32 UNF thread, Nylon, 25/pk	Cole-Palmer	UX-45502-60
Firefly MV 0.3 MP Mono USB 2.0	Point Grey	FMVU-03MTM-CS
Mastech Regulated Variable Linear DC Power Supply	Mastech	HY3003D

LEAD CONTACT AND MATERIALS AVAILABILITY

Further information and requests for resources and reagents should be directed to and will be fulfilled by the Lead Contact, Vanessa Ruta (ruta@rockefeller.edu).

EXPERIMENTAL MODEL AND SUBJECT DETAILS

Fly strains

Fly strains and husbandry

Flies used for *ex vivo* brain explant preparations and functional imaging using chemogenetic and shock activation of DANs were maintained on conventional cornmeal-agar-molasses at 25°C and 60%–70% relative humidity, under a 12 hr light:12 hr dark cycle. Flies used for optogenetic behavioral experiments were maintained at 25°C and 60%–70% relative humidity in constant darkness. For optogenetic experiments, 1-3 day old females were transferred to cornmeal-agar-molasses food containing 0.4 mM all trans-Retinal (Sigma #R2500) and reared in the dark for 2-3 days before behavioral experiments. Flies were not food-deprived prior to any functional or behavioral experiments.

Generation of ER-GCaMP transgenic flies

The coding sequence for the low-affinity ER calcium sensor (ER-GCaMP6-210) (de Juan-Sanz et al., 2017) containing an N-terminal calreticulin signaling peptide and C-terminal KDEL ER retention sequence was PCR amplified using KOD Hot Start DNA polymerase. Restriction sites were added to the 5′ and 3′ end of the coding sequence (*XhoI* and *XbaI*, respectively). The amplified product and pJFRC81 (Addgene Plasmid #36432) were digested with *XhoI* and *XbaI* and ligated together. The resulting plasmid was used to generate transgenic flies by PhiC31 mediated integration into VK00005 and attp5 (Bestgene Inc.).

Crispr-Cas9 mediated deletion of DopR1

Existing DopR1 mutants were generated either imprecisely using a larger chromosomal inversion (dumb[1], Kim et al., 2007), through disruption by a transposable PiggyBac element and therefore incompatible with 2-photon imaging (*dumb*[2], Kim et al., 2007), or were actually hypomorphs (Keleman et al., 2012) based on immunohistochemistry. We therefore generated a novel DopR1 mutant compatible with functional imaging. Two gRNAs were designed to direct Cas9-mediated cleavage to the 5′ and 3′ UTRs of the *Dop1R* gene locus. gRNA off-target potential was determined using Crispr optimal target finder (http://targetfinder.flycrispr.neuro.brown.edu) gRNA sequences were PCR amplified with Q5 High-Fidelity master mix (NEB) and cloned into pCFD4 by Gibson assembly (NEB). The resulting vector was sequence verified and injected into nos-Cas (Bloomington stock 54591) embryos (Rainbow Transgenic Flies). G0 flies were individually crossed to a balancer strain prior to being screened for the deletion by PCR-based genotyping. Each G0 founder positive for the deletion was further verified by Sanger sequencing. F1 progeny from a deletion positive G0 parent were individually crossed to a balancer strain then screened for transmission of the deletion. Multiple unique deletion lines were obtained and a single line was then used for further experimentation. Loss of DopR1 protein expression in the mutant was verified by immunohistochemistry with anti-DopR1 antibody (a gift from Tim Lebetsky) and qRT-PCR in adult fly brains.

Detailed fly genotypes used by figure

Figures 1A–1G, S1B–S1J, S2B–S2J, 2A, 2B, 3B–3D, and S4B–S4D:

w^{1118} UAS-CsChrimson.mVenus; R58E02-p65.AD (PAM DAN split); R22E04-Gal4.DBD (PAM DAN split)
w^{1118} UAS-CsChrimson.mVenus; 52H03-p65.AD (PPL DAN split); TH-Gal4.DBD (PPL DAN split)
w^{1118} UAS-CsChrimson.mVenus

Figures 2C–2E, S3A, S3B, 3E, 3F, S4E, S4F, 6E, and S7D:

R58E02-LexA (γ4-5 DANs), LexAOP-P2X$_2$; VT026001-Gal4 (γ4 MBON), UAS-GCaMP6s

Figure S3C:

R58E02-LexA (γ4-5 DANs), LexAOP-P2X$_2$/ UAS-GCaMP6s; 66C08-Gal4 (γ5 MBON)

Figure S3D:

73F07-LexA (γ2 DANs)/LexAOP-P2X$_2$; 25D01-Gal4 (γ2 MBON), UAS-GCaMP6s

Figure S3E:

25D01-LexA (γ2 MBON), LexAOP-GCaMP6s

Figures 4A–4 and S5A–S5G:

w^{1118}; R58E02-p65.AD (PAM DAN split)/53C03-LexA (γ4 MBON), LexAOP-GCaMP6s; R22E04-Gal4.DBD (PAM DAN split)/UAS-ChrimsonR.mCherry

Figures 5A and S6A:

R58E02-LexA (γ4-5 DANs), LexAOP-P2X$_2$; LexAOP-GCaMP6s

Figures 5B and S6B:

R58E02-LexA (γ4-5 DANs), LexAOP-P2X$_2$; TH-Gal4 (DAN subset), DDC-Gal4 (DAN subset)/UAS-VMAT-pHluorin

Figures 5C, S6C, and S6D:

R58E02-LexA (γ4-5 DANs), LexAOP-P2X$_2$; UAS-GRAB$_{DA1m}$; OK107-Gal4 (KCs)

Figures 5D, 5E, S6E, S6G, 6A, and 6B:

R58E02-LexA (γ4-5 DANs), LexAOP-P2X$_2$; UAS-EPAC (cAMP); OK107-Gal4 (KCs)

Figures 5D, 5E, S6F, S6H, 6C, 6D, and S7C:

R58E02-LexA (γ4-5 DANs), LexAOP-P2X$_2$; UAS-ER-GCaMP-210; OK107-Gal4 (KCs)

Figures 6A and 6B:

R58E02-LexA (γ4-5 DANs), LexAOP-P2X$_2$/UAS-EPAC (cAMP); DopR1^{null}/DopR1^{null}; OK107-Gal4 (KCs)
R58E02-LexA (γ4-5 DANs), LexAOP-P2X$_2$/UAS-EPAC (cAMP); DopR2^{attP}/DopR2^{attP}; OK107-Gal4 (KCs)
R58E02-LexA (γ4-5 DANs), LexAOP-P2X$_2$; UAS-EPAC (cAMP); OK107-Gal4 (KCs)

Figures 6C and 6D:

R58E02-LexA (γ4-5 DANs), LexAOP-P2X$_2$/UAS-ER-GCaMP-210; DopR1^{null}/DopR1^{null}; OK107-Gal4 (KCs)
R58E02-LexA (γ4-5 DANs), LexAOP-P2X$_2$/UAS-ER-GCaMP-210; DopR2^{attP}/DopR^{attP}; OK107-Gal4 (KCs)
R58E02-LexA (γ4-5 DANs), LexAOP-P2X$_2$; UAS-ER-GCaMP-210; OK107-Gal4 (KCs)

Figures 6E–6G:

R58E02-LexA (γ4-5 DANs), LexAOP-P2X$_2$/UAS-GCaMP6s; VT026001-Gal4 (γ4 MBON), DopR1^{null}/ VT026001-gal4 (γ4 MBON), DopR1^{null}
R58E02-LexA (γ4-5 DANs), LexAOP-P2X$_2$/UAS-GCaMP6s; VT026001-Gal4 (γ4 MBON), DopR2^{attP}/ VT026001-gal4 (γ4 MBON), DopR2^{attP}
R58E02-LexA (γ4-5 DANs), LexAOP-P2X$_2$; VT026001Ggal4 (γ4 MBON), UAS-GCaMP6s

Figures 7A–7D, S8A–S8D, and S8F–S8S:

w^{1118}; R58E02-p65.AD (PAM DAN split)/ UAS-CsChrimson.mVenus; R22E04-Gal4.DBD (PAM DAN split)
w^{1118}; R58E02-p65.AD (PAM DAN split)/ UAS-CsChrimson.mVenus; R22E04-Gal4.DBD (PAM DAN subset), DopR1^{null}/ R22E04-ZpGdbd (PAM DAN split), DopR1^{null}
w^{1118}; R58E02-p65.AD (PAM DAN split)/ UAS-CsChrimson.mVenus; R22E04-Gal4.DBD (PAM DAN split), DopR2^{attP}/R22E04-ZpGdbd (PAM DAN subset), DopR2^{attP}

METHOD DETAILS

Functional imaging

All functional imaging experiments were performed on an Ultima two-photon laser scanning microscope (Bruker Nanosystems) equipped with a Chameleon Ultra II Ti:Sapphire laser. The excitation wavelength was 920 nm for all experiments except for FRET imaging of the EPAC sensor, which was excited at 850 nm. Emitted fluorescence was detected with either photomultiplier-tube or GaAsP photodiode (Hamamatsu) detectors. Images were acquired with an Olympus objective, either 40X, 0.8 NA or 60X, 1.0 NA at 512 × 512 pixel resolution. Quantification of neural activity was performed by normalizing fluorescence intensity changes (ΔF/F) or CFP/YFP fluorescence ratio changes (ΔR/R) to control for variations in reporter expression and imaging parameters across neurons and experiments. ROIs were manually drawn using anatomic landmarks. The inter-stimulus interval between KC stimulation or odor presentation and DAN activation during conditioning was calculated by subtracting the onset of KC stimulation/odor presentation (time zero) from the onset of DAN activation.

In *ex vivo* experiments, brains from 1-4 day old male or female flies were dissected in saline (108 mM NaCl, 5 mM KCl, 2 mM $CaCl_2$, 8.2 mM $MgCl_2$, 4 mM $NaHCO_3$, 1 mM NaH_2PO_4, 5 mM trehalose, 10 mM sucrose, 5 mM HEPES, pH 7.5 with osmolarity adjusted to 265 mOsm), briefly (45 s) treated with collagenase (Sigma #C0130) at 2 mg/mL in saline, washed with fresh saline, and then pinned with fine tungsten wires to a thin Sylgard sheet (World Precision Instruments) in a 35 mm Petri dish (Falcon) filled with saline. For *in vivo* imaging experiments in which we examined odor-specific modulation of γ4 MBON responses (Figure 3F, S4E, and S4F), 1-4 day old female flies were prepared as described previously (Cohn et al., 2015). For *in vivo* imaging experiments in which we examined odor-specific modulation of odor and behavioral responses in the closed-loop assay (Figures 4 and S5), flies were prepared as described previously (Green et al., 2017) with minor modifications. Briefly, 3-5 day old female flies were temporarily anesthetized using CO_2 (for < 60 s) while tethering to a milled plastic holder (Green et al., 2017) using UV-curable glue (Loctite) applied to each eye and thorax. The proboscis was glued in an extended position to minimize brain motion during imaging. The dish was then filled with saline and the cuticle covering the dorsal portion of the head was removed. Muscle 16 and obstructing trachea were removed. Care was taken to keep the antennae and antennal nerves intact. On rare occasions, flies showed no movement or odor responses and were discarded.

Imaging in *ex vivo* brain explants

(Figures 2D, 2E, S3A–S3D, 5A–5E, S6A–S6H, 6A–6G, S7C, and S7D)

Stimulation of Kenyon Cells

Stimulation of Kenyon Cell dendrites was performed as described previously (Cohn et al., 2015). Briefly, glass-stimulating electrodes were pulled to a resistance of 7–10 MΩ and filled with 10 mM acetylcholine (Sigma) in saline. Stimulating electrodes were positioned into the mushroom body calyx viewed under IR-DIC optics. Square voltage pulses (500 ms, 0.1-15V for all imaging experiments) were used to iontophorese acetylcholine into the calyx and excite Kenyon Cells. Pulse trains were generated by a stimulator (Grass Technologies) triggered by Prairie View software. The inter-trial interval for calycal stimulations was at least 20 s to assure activity levels returned to baseline. On the rare occasion that MBON responses could not be evoked or were unusually variable in the absence of conditioning, the mushroom body in other hemisphere of the brain was tested or the prep was discarded.

Activation of DANs expressing $P2X_2$

To chemogenetically stimulate DANS in explant experiments (Figures 2D, 2E, S3A–S3D, 5A–5E, S6A–S6H, 6A–6G, S7C, and S7D), R58E02-LexA or 73F07-LexA was used to drive expression of the $P2X_2$ channel in either the PAM DANs or γ2 DAN, respectively. Glass stimulating electrodes pulled to a resistance of 7-10 MΩ were filled with 2 mM ATP in saline and positioned dorsal to the mushroom body's medial lobes, in the superior medial protocerebrum (Cohn et al., 2015) at the site of rich DAN dendritic innervation. To validate that placement of the electrode in the superior medial protocerebrum drove activation of DANs, in a subset of experiments, responses of DANs expressing GCaMP were directly measured. DANs were stimulated using a train of five 100-ms pulses at 2.5-5V with an inter-pulse interval of 20 ms. Trains were generated by a stimulator (Grass Technologies) that was triggered by Prairie View software. The inter-trial interval following DAN activation was at least 20 s.

Modulation of KC-MBON signaling

KC-evoked responses in the γ2, γ4, and γ5 MBON were measured as the peak fluorescence evoked in the 2 s following KC stimulation, normalized to baseline fluorescence (2-3 s prior to KC stimulation). To compare KC-evoked calcium responses in the γ2, γ4, and γ5 MBON prior to and after conditioning (Figures 2D, 2E, S3C, S3D, 6E–6G, and S7D), two responses to KC stimulation prior to pairing were averaged ('pre') and two responses to KC stimulation after pairing were averaged ('post') to control for any potential inter-trial variability. To calculate the change in KC-evoked response in the MBONs due to conditioning in Figure 2E, S3C, and S3D, the peak fluorescence response prior to pairing was subtracted from the response post pairing as schematized in Figure 2D.

To examine bidirectional modulation of γ4 and γ5 MBON experiments in Figures S3A–S3C and 6E–6G or γ2 MBON in Figure S3D, the inter-stimulus intervals (ISI, DAN onset minus KC onset) used for conditioning were optimized to elicit the most robust plasticity. In some explant preparations in Figures S3C and S3D, each mushroom body was treated as an independent sample. Each data point in Figures 2D, 2E, S3C, S3D, 6E–6G, and S7D represents plasticity evoked by a single conditioning trial within an independent sample. In Figures S3A and S3B, where forward and backward pairing were performed within the same preparation, individual KC-evoked γ4 MBON responses were plotted over time prior to and following conditioning trials. To examine deficits in γ4 MBON plasticity in dopamine receptor mutants (Figures 6E–6G), wild-type and receptor mutant preparations were interleaved. The GCaMP responses of the

γ4 MBON in DopR2 mutants exhibited higher fluctuations than typically observed in wild-type animals but these were averaged out across experiments and did not obscure KC-evoked responses.

Imaging of fluorescent reporters in KC and DAN axons

To quantify ER calcium release in the γ4/γ5 compartments of KC axons (OK107-Gal4 > UAS-ER-GCaMP-210) during conditioning, we averaged the response for 1 s following KC activation (Figures 5D, 5E, 6C, 6D, and S7C) to account for the rapid kinetics of this signal, the fact that ER calcium release was time-locked to KC stimulation, and its relatively low signal to noise (Figure S6H). ER-GCaMP fluorescence was normalized by the mean intensity for 2-4 s prior to KC stimulation.

The $GRAB_{DA1m}$ sensor was expressed in KC axons using the cell-type specific OK107-Gal4. TH,DDC-Gal4 driver was used to express VMAT-pHluorin in DANs and the 58E02-LexA driver was used to express GCaMP6s in the γ4/γ5 DANs. VMAT-pHluorin, $GRAB_{DA1m}$, and TH,DDC traces exhibited a higher signal than ER-GCaMP, enabling us to use the peak response evoked in the γ4/γ5 compartments during conditioning (Figures 5A–5C and S6A–S6C). VMAT-pHluorin, $GRAB_{DA1m}$, and GCaMP6s responses were normalized by the mean intensity for 2-4 s prior to stimulation.

Ratiometric imaging of the FRET-based cAMP sensor, EPAC, was measured in the γ4/γ5 KC axon segments (OK107-Gal4 > UAS-EPAC) during conditioning (Figures 5D, 5E, S6G, 6A, and 6B). A Semrock filter set (#FF506-Di03-25x36, #FF01-483/32-25, #FF01-534/30-25) was used to spectrally separate and monitor CFP and YFP emission and responses were imaged at 850 nm. The CFP/YFP ratio was measured for each frame with an increase in this ratio corresponding to increased cAMP levels. To measure cAMP evoked during conditioning, we averaged the CFP/YFP ratio for the 4 s following DAN activation to account for the slow kinetics of this signal and the fact that cAMP was produced under all conditions and in response to direct DAN activation (Figure S6G). The DAN-evoked CFP/YFP fluorescence was normalized to the CFP/YFP ratio in the 2-4 s prior to stimulation.

In Figures S6D–S6F, evoked levels of dopamine release ($GRAB_{DA1m}$), cAMP (EPAC), and ER calcium release (ER-GCaMP) in the KC axons (OK107) in the proximal γ2/γ3 compartments and the PAM-innervated γ4/γ5 compartments were measured during conditioning as described above to assess local production of second messengers along KC axons. For this comparison aggregated cAMP and ER calcium data from wild-type animals in Figures 5D, and 6A, and 6C, and the data of dopamine levels in KCs from Figure S6C were re-analyzed to compare fluorescent responses across the distal (γ2/γ3) and proximal (γ4/γ5) compartments of the γ lobe. Compartmental boundaries were determined using anatomic landmarks. For Figures 5A–5E, S6A–S6D, S6G, S6H, 6A–6D, and S7C all pairing conditions were tested in each brain preparation, and the order of pairing conditions tested was varied across experimental preparations. In Figure 5F, cAMP and ER calcium responses from Figure 5E were normalized by the minimal and maximal responses to determine the relative second-messenger signaling as a function of the ISIs used in conditioning. We then subtracted the normalized cAMP signal from the normalized ER calcium signal, based on the assumption that these pathways work in opposition to one another to regulate synaptic plasticity as indicated by the selective deficits in plasticity observed in the dopamine receptor mutants. The standard error of the mean of cAMP and ER calcium responses were propagated.

YM-254890 (Gαq inhibitor) drug treatment

The Gαq inhibitor, YM-254890 (Wako Chemicals #257-00631), was applied (10 μM in DMSO) to the saline bathing an explant preparation. Control experiments using saline with equivalent amounts of DMSO were interleaved with drug treatments to test the effect of YM-254890.

Behavioral experiments in laminar flow chambers

(Figures 1B–1G, S1A–S1J, S2B–S2J, 2A, 2B, 3B–3D, S4B–S4D, 7A–7D, and S8A–S8S)

Chamber construction

Fly chamber component pieces were cut from acrylic sheets using a laser cutter. The lid and base of each chamber were cut from transparent acrylic (Clear Cast Acrylic Sheet, 12'' x 24'' x 1/16,'' McMaster Carr). Two holes on opposite sides of the lid were tapped for 10-32 threaded Luer lock connectors. A single hole was cut in the base to allow flies to be loaded and unloaded. A spacer was cut from a 3-mm black scratch-resistant acrylic sheet (McMaster-Carr) with a central empty chamber (20 mm x 50 mm) flanked by two manifolds. Narrow channels were etched between the manifolds and central chamber using a low-power setting of the laser cutter. This permitted airflow between the chamber and the manifolds while confining flies within the chamber. The dimensions of the inside chamber were 20 mm x 50 mm x 3 mm. The base, spacer, and lid were glued together using acrylic solvent and the edges of the chamber were further sealed with epoxy (Devcon 5 Minute® Epoxy) to make them airtight. 10-32 Luer connectors were screwed into the top of the chamber and sealed around the edges with epoxy.

Behavioral set-up

Flies in chambers were assayed in a custom-built training and testing rig. Chambers were placed on a 3-mm thick acrylic sheet suspended on aluminum posts above a 3 × 4 array of 627 nm LEDs (Luxeon Rebel). LEDs were attached to metal heat sinks (Mouser #532-374624B32G), which were secured at 5 cm intervals to a 30 × 30 cm aluminum wire cloth sheet (McMaster-Carr #9227T53). LEDs were driven by Recom Power RCD-24-0.70/W/X2 drivers, which were powered by a variable DC power supply. Infrared LED strips (940 nm, LED Lights World) attached to the wire cloth between the heat sinks provided back-illumination of the platform. A Firefly camera (Point Grey) was mounted in a central hole within an acrylic lid suspended 30 cm above the platform on aluminum posts. Flies were recorded at 30 frames/s. Odor presentation and airflow were controlled using 3-way micro solenoid valves. A vacuum line was used to draw air into each chamber at a rate of 0.75-1.25 L/min/chamber. Two valves were used to control the direction of airflow, and additional valves were used to switch between clean air and different odors. Valves were powered by a 12 V DC power

supply and switched on and off using VO14642AT solid state relays. Chamber design and valve system are shown in Figure S1A. Valve relays and LED drivers were controlled by the output pins of an Arduino running custom software. Custom software written in C was used for data acquisition and instrument control during individual trials of odor/light presentation. Python scripts were used to execute sequences of trials.

Odor stimulation

Odorants were placed in glass bottles with lids containing two Luer connectors. One connector was attached to an odor inlet valve and the other was left open to allow room air to enter the bottle. By default, air entered the apparatus through a bottle containing distilled water. To deliver odor pulses, the solenoid valve to the water bottle was closed while simultaneously opening the valve to an odor bottle. The valves were then switched back to their resting position after the specified odor presentation interval (Figure S1A).

For each baseline, post-forward pairing, and post-backward pairing trial, animals experienced two odor presentations for each odor tested—one presentation originating from the top of the chamber the other originating from the bottom. The air-flow direction across the chamber was switched 19 s prior to odor onset and 20 s after odor offset. The mean upwind displacement for the group of flies for the two odor presentations originating from the top and bottom of the chamber was used to assess odor-tracking behavior for each trial. This was done to control for any variability in air/odor flow between the two chamber sides. All training trials lasted 11.6 s except for training trials in Figures 2A and 2B, which lasted 20 s to accommodate the longer inter-stimulus intervals between LED and odor presentation. Testing trials began 60 s after a training trial.

Pure apple cider vinegar (Heinz) was used for testing and training for experiments in Figures 1B–1G, S1B–S1J, S2B–S2J, 2A, 2B, 7A–7D, and S8A–S8S. The two odorants used in Figures 3A–3D and S4A–S4C to test for odor-specific behavioral modulation were isobutyl acetate (odor 1) and 4-methylcyclohexanol, *cis+trans* (odor 2); the two odors used in Figure S4D were benzaldehyde (odor 1) and 1-hexanol (odor 2). All monomolecular odors were diluted 1:1000 in heavy mineral oil. All odor presentations were 2 s in duration.

Optogenetic activation of DANs

PPL and PAM DANs expressing the light sensitive ion channel, CsChrimson, were activated using 1 s illumination with 627 nm LEDs. Split-Gal4s were used to drive CsChrimson in either the PAM cluster (MB042B) or PPL cluster (MB504B) DANs. The intensity of light within each chamber during LED illumination was approximately 18-40 $\mu W/mm^2$.

Associative conditioning

4-7 flies were loaded into each chamber through the bottom port using a mouth pipette. The exact number of flies used per experiment is referenced in the table below. The bottom port was sealed with a piece of transparent Scotch tape after loading. Chambers were aligned in an acrylic frame on the imaging platform and connected in parallel to air inlets using Tygon tubing.

To examine how odor tracking was altered from a single forward pairing (FP) conditioning trial (Figure S1B), PPL > Chrimson animals experienced five baseline trials followed by a single forward pairing trial in which apple cider vinegar (ACV) was presented for 2 s, and LED illumination was provided during the final second of odor presentation. Animals then experienced 15 odor test trials to assess the time course of memory decay. To assess the ability of backward pairing (BP) to reverse a negative association following forward pairing (Figure S1C), PPL > Chrimson animals were conditioned as described above, however, after a single odor test trial, animals were conditioned by backward pairing in which the onset of a 1 s pulse of LED illumination preceded ACV presentation by 2 s. Animals then experienced 14 odor test trials post-BP to examine the decay in the memory formed by backward pairing. To examine the effect of a single backward pairing trial on nominally naive PAM > Chrimson flies, the baseline upwind displacement in a single odor trial was compared to the displacement in the first test odor trial immediately following a single backward pairing conditioning trial (Figure S1F).

For experiments examining how behavioral tracking was modulated by interleaving forward pairing and backward pairing (Figures 1B–1G, S1D, S1E, S1I, S1J, S2B–S2J, 7A–7D, and S8A–S8D), animals were conditioned as above but with 25 training trials of forward pairing and 25 trials of backward pairing interleaved between test trials. To assess whether odor re-exposure or DAN re-activation alone (Figures S1G–S1J) could erode forward pairing associations to the same extent as backward pairing, 25 forward pairing trials were interleaved with 25 trials with the same timing as backward pairing but with either the odor or DAN stimulation omitted.

To examine how varying the inter-stimulus interval (ISI) of odor and DAN stimulation during conditioning altered behavioral tracking (Figures 2A and 2B), five different ISIs were tested with 10 trainings of each interleaved in a random order over the course of an experiment. The randomization of ISI tested was used to account for any dependence on the trial structure.

To examine how a single reinforcement can instruct multiple odor-specific associations (Figures 3A–3D and S4A–S4D), we trained flies with two monomolecular odorants which were sequentially presented in each baseline, post-FP, and post-BP trial. During the conditioning trials, each odorant was presented for 2 s with a 1 s inter-stimulus interval of clean air. PAM > Chrimson activation began 1 s after the start of the first odor presentation and 2 s prior to the presentation of the second odor. Experiments consisted of 25 training trials in which odor 1 was forward paired and odor 2 was backward paired and 25 training trials in which odor 2 was forward paired and odor 1 was backward paired. Training trials in which odor 1 was forward paired and odor 2 was backward paired were interleaved with training trials where odor 2 was forward paired and odor 1 was backward paired.

To compare baseline locomotor parameters and odor tracking behavior in nominally naive wild-type and dopamine receptor mutant PAM > Chrimson animals (Figures S8E–S8S), responses to ACV were measured over 9 odor trials, with each odor trial consisting of one odor presentation originating from the top of the chamber and one originating from the bottom as described above. Various behavioral metrics of wild-type, $DopR1^{-/-}$, and $DopR2^{-/-}$ animals prior to and during the odor were compared across genotypes. Analysis of behavioral metrics is described below.

All experiments were performed in the dark. Chambers were cleaned at the beginning or end of each experimental day by using a syringe to flush them thoroughly with water followed by 70% ethanol. Chambers were not cleaned between experiments within the same day; no difference in behavior was observed across subsequent experiments within the same day when testing with the same conditioning paradigm. Behavioral responses to ACV were often variable in the first 1-2 baseline trials and were discarded from analysis to assure a stable readout of nominally naive attraction.

Tracking of fly trajectories and behavioral analysis

(Figures 1B, S2B–S2J, and S8F–S8S)

The trajectories of individual flies were tracked across trials to examine how behavioral metrics were altered as a result conditioning (Figures S2B–S2J), or to compare locomotor characteristics of wild-type, DopR1$^{-/-}$, and DopR2$^{-/-}$ animals (Figures S8F–S8S) by capturing movies of flies throughout the trial. A background image was generated by taking the maximum value of each pixel over the entire movie. To account for fluctuations in illumination intensity, this background image was rescaled frame-by-frame by the average pixel intensity. After subtracting the rescaled background, the image was bandpass-filtered, and flies were detected with a local maximum-finding algorithm (derived from the function pkfnd.m, which can be found at http://site.physics.georgetown.edu/matlab/code.html). Centroid positions of flies were then calculated from the original background-subtracted image using the function cntrd.m (http://site.physics.georgetown.edu/matlab/code.html). Fly localizations from individual frames were combined into multi-frame tracks using the function track.m (http://site.physics.georgetown.edu/matlab/code.html). The Y-axis and X-axis were defined as the axes parallel or perpendicular to the air/odor stream, respectively. For Figures S2B–S2J and S8F–S8S, X and Y speeds were defined as the absolute values of the velocity components in the X and Y directions. To examine Y-speed exclusively in moving animals a threshold of > 1 pixel/s (0.3 mm/s) was used to identify walking animals. The fraction of stationary flies was defined as the proportion of animals moving < 0.3 mm/s; the fraction of animals walking sideways was defined as the proportion of flies moving > 0.3 mm/s and within ± 45 degrees of the X axis; and the fractions of animals walking upwind or downwind were defined as the proportions of animals moving > 0.3 mm/s and within ± 45 degrees of the positive or negative Y axis, respectively.

Center of mass tracking

(Figures 1C–1G, S1B–S1J, 2A, 2B, 3B–3D, S4B–S4D, 7A–7D, and S8A–S8D)

To measure the aggregate behavior of groups of flies, background subtraction was performed as above, and background noise was further suppressed by setting to zero all pixels below an empirically determined threshold. The same threshold was applied to all chambers in an experiment depending on background illumination to improve tracking accuracy. The centroid position of all flies was then calculated for each background-subtracted frame. Upwind center-of-mass velocities were smoothed using a 15-frame moving average across each testing trial. The upwind velocity raster plots for each trial show animal behavior over an 11 s time window with odor on between 4-6 s. Upwind displacement during odor presentation was defined as the difference in center-of-mass position along the airflow direction between time of odor onset and time of odor offset. Change in upwind displacement after conditioning was calculated by subtracting the upwind displacement in the trial immediately preceding the conditioning trial from the upwind displacement in the trial immediately following the conditioning trial. This was done for all conditioning trials across each experiment. The mean change in upwind displacement across all training trials of the same training paradigm in an experiment was used to compare behavioral modulation across different conditioning paradigms and genotypes. Positive changes in upwind displacement indicate increased upwind odor tracking and negative changes indicate decreased upwind odor tracking. To compare upwind displacement after a single forward-paired or backward-paired conditioning trial (Figures S1B, S1C, and S1F) the raw upwind displacement values in the center of mass of flies in odor trials immediately preceding and following conditioning were compared to assess the effects of conditioning. In Figure S1B the upwind displacement in the first two odor trials following forward pairing were compared to assess initial memory decay. For dopamine receptor mutants (Figures S8C and S8D), the raw upwind displacement values in the center of mass of flies post-forward pairing and post-backward pairing were compared between wild-type and mutant animals. The total number of experiments and flies used in the laminar airflow system is listed below with related Figure references on the left.

Figure	Genotype	Experiments (N)	Total flies
Figures 1D–1G and S2B–S2J	PAM (MB042B) > CsCh	8	48
Figures 1D–1G and S2B–S2J	PPL (MB504B) > CsCh	8	48
Figure S1B	PPL (MB504B) > CsCh	11	66
Figure S1C	PPL (MB504B) > CsCh	11	66
Figure S1D and S1E	CsCh	8	48
Figure S1F	PAM (MB042B) > CsCh	8	44
Figures S1I and S1J	PAM (MB042B) > CsCh (FP-BP experiment)	7	43
Figures S1I and S1J	PPL (MB504B) > CsCh (FP-BP experiment)	7	42
Figures S1G, S1I, and S1J	PAM (MB042B) > CsCh (FP-Odor Alone)	7	42
Figures S1G, S1I, and S1J	PPL (MB504B) > CsCh (FP-Odor Alone)	8	48

(*Continued on next page*)

Continued

Figure	Genotype	Experiments (N)	Total flies
Figures S1H–S1J	PAM (MB042B) > CsCh (FP-DAN Alone)	8	48
Figures S1H–S1J	PPL (MB504B) > CsCh (FP-DAN Alone)	8	48
Figures 2A and 2B	PAM (MB042B) > CsCh	6	34
Figures 2A and 2B	PPL (MB504B) > CsCh	6	34
Figures 2A and 2B	CsCh	7	38
Figures 3A–3C	PAM (MB042B) > CsCh	8	48
Figures S4A–S4C	CsCh	7	42
Figure S4D	PAM (MB042B) > CsCh	11	55
Figure S4D	CsCh	9	45
Figures 7A, 7C, S8A, and S8C	PAM (MB042B) > CsCh (controls for DopR1$^{-/-}$)	7	42
Figures 7A, 7C, S8A, and S8C	PAM (MB042B) > CsCh, DopR1$^{-/-}$	7	42
Figures 7B, 7D, S8B, and S8D	PAM (MB042B) > CsCh (controls for DopR2$^{-/-}$)	7	37
Figures 7B, 7D, S8B, and S8D	PAM (MB042B) > CsCh, DopR2$^{-/-}$	7	42
Figures S8F–S5S	PAM (MB042B) > CsCh	4	20
Figures S8F–S5S	PAM (MB042B) > CsCh, DopR1$^{-/-}$	4	20
Figures S8F–S5S	PAM (MB042B) > CsCh, DopR2$^{-/-}$	4	20

Conditioning with multiple odors in tethered flies

(Figures 3E, 3F, S4E, and S4F)

Tethered flies were stimulated with odor by directing a continuous stream (400 mL/min) of clean air through a 2 mm diameter teflon tube directed at the fly's antenna (carrier stream). 5% of the total airstream was diverted through the headspace of either an empty or odor filled 10 mL glass vial (odor stream). At a trigger, a custom-built solenoid valve controller system redirected the odor stream from the empty vial to the vial containing various odorants diluted 1:10 in heavy mineral oil (Sigma). The odorants used in Figure 3F were isobutyl acetate (odor 1) and *cis*+trans 4-methylcyclohexanol (odor 2). The odorants used in Figure S4E were 1-hexanol and benzaldehyde. For half of the experiments in Figure S4E, 1-hexanol was odor 1 and benzaldehyde was odor 2; for the other half of experiments the odor identities were reversed. Each odor presentation was 2 s in duration. Each odor was presented 2-4 times during baseline and post-pairing trials and the responses in the γ4 MBON for each odor were averaged. Odor-evoked responses in the γ4 MBON were normalized by the mean fluorescence for 10 s prior to odor presentation. In Figures 3F, S4E, and S4F, 58E02-DANs expressing the $P2X_2$ channel were activated as described above. During conditioning trials, the two odors were each presented for 2 s. DANs were stimulated using four 100-ms pulses at 5V with an inter-pulse interval of 20 ms. The DAN stimulation started 1.5 s after the start of the first odor presentation and 1.7 s prior to the presentation of the second odor. The delay between odor 1 and odor 2 during conditioning was 1.2 s. The presentation order of odor 1 and odor 2 during conditioning was alternated between subsequent conditioning trials. Odor-evoked responses were measured by taking the peak fluorescence during the 2 s odor presentation. To compare the odor-specific modulation in the γ4 MBON across odor pairs (Figure S4F), the mean peak response for each odor prior to a conditioning paradigm was subtracted from the mean peak response for each odor immediately post pairing; the change in evoked responses for odor 1 and odor 2 following conditioning were compared. The animals plotted in Figures 3F and S4E had experienced prior conditioning in which odor 1 was backward paired and odor 2 was forward paired. The inter-trial interval between all odor presentations and conditioning trials was at least 20 s.

Conditioning with electric shock in tethered flies

(Figure S3D)

Animals were tethered to a holder as above (Green et al., 2017) but modified to include a polypropylene Luer with a 2 mm opening directed at the antenna of the fly for odor delivery. Odor stimulation was performed as described above, however, in these experiments 40% of the total airstream was diverted through the headspace of a glass vial filled with pure ACV to ensure consistent responses in the γ2 MBON. ACV was presented twice to each fly in baseline, post-FP, and post-BP trials and were normalized and averaged as described above. If the γ2 MBONs in both hemispheres were visible in the same imaging plane, odor-evoked responses from both output neurons were averaged together. After positioning the fly under the microscope, two copper washers were precisely placed under visual control to make contact with either side of the fly's abdomen. Electrical leads from the two washers were connected to a stimulator (Grass Technologies), which was used to apply two 1 s shocks of 70 V that were separated in time by a 200 ms delay. In forward pairing trials, odor onset preceded shock onset by 500 ms. In backward pairing trials, the onset of shock preceded odor onset by 3 s. The mean peak response in the γ2 MBON immediately prior to a conditioning trial was subtracted from the response following either forward or backward pairing to assess the change in odor-evoked responses as a consequence of conditioning. The inter-trial interval between all odor presentations and conditioning trials was at least 20 s.

Behavioral and functional imaging in closed-loop system

(Figures 4 and S5)

Closed-loop system

An air-supported foam ball (~6.5 mm diameter, Matsubara Sangyo Co.) was modified based on prior work (Green et al., 2017; Seelig and Jayaraman, 2015) and positioned within the fly's grasp to allow the fly to 'walk' on the ball during imaging. On the rare occasion an animal could not maintain control of the ball because of its placement on the ball, the trial was discarded. The ball was recorded at 60-61 fps using a Point Grey Firefly Camera with Infinity Lens (94 mm focal length) focused on the ball, which was illuminated by infrared LED lights. Ball rotation was calculated in real time using FicTrac software (Moore et al., 2014) running on Ubuntu 12.04 on computers with processors with speeds of at least 3GHz. The heading of the fly, as calculated by FicTrac, was transmitted to an Arduino Mega via serial port. Custom Arduino code was used to translate heading into tube position controlled by motors described below.

The closed loop air-delivery system was custom designed using OnShape (https://www.onshape.com) and 3D printed using Visijet Crystal material at XHD resolution in a 3DSystems Projet 3510 HD Plus. O-ring OD and ID Gland surfaces were designed with excess material for printing then manually modified on a lathe for improved RMS [surface] finishing. Tube rotation over 360 degrees was driven by a bipolar stepper motor (Pololu #1206) controlled through a A4988 Stepper Motor Driver Carrier (Pololu #2980) coupled by a Dust-Free Timing Belt XL Series, 1/4'' Width (McMaster-Carr, 1679K121, Trade No. 130xL025) to the rotating tube system, which rotated mounted on an Ultra-Corrosion-Resistant Stainless Steel Ball Bearing (3/4'' Shaft Diameter, 1-5/8'' OD, Mcmaster-Carr 5908K19). Air channel was kept airtight using oil resistant o-rings (1/16 Fractional Width, Dash Number 020, Mcmaster-Carr 2418T126). Motor rotation was measured by a rotary encoder (CUI Inc., AMT10 Series) that was used in order to correct for skipped steps.

Odor stimulation in walking flies in the closed loop system

Odor stimulation was achieved by directing a continuous stream (400 mL/min) of clean air through a 2 mm diameter tube made of Visijet Crystal material directed at the fly's antenna. 20% of the total airstream was diverted through the headspace of a 500 mL glass bottle containing water. At a trigger, a custom-built solenoid valve controller system redirected the odor stream from the water bottle to a bottle containing pure ACV. A 10 s odor presentation was used to allow the fly time to respond to and track the odor. Shorter odor presentations led to less consistent tracking in naive animals, potentially due to the need to compensate for the inertia of the ball. In baseline and test trials after forward pairing and backward pairing, animals were presented with two 10 s ACV odor presentations separated by 30 s of clean air. The peak odor-evoked fluorescence in the γ4 MBON and the total upwind displacement in ACV for the two 10 s odor presentations were averaged together for baseline and test trial measurements. Odor responses in the γ4 MBON were normalized by the mean intensity of the GCaMP signal in the 10 s prior to the first odor presentation in each baseline and test trial. The odor-evoked responses in the γ4 MBON in both hemispheres were averaged for analysis except in one preparation where the γ4 MBON was visible in only one hemisphere. Due to a small latency in image capture rate, a systematic delay was introduced in image sequences between baseline, post-forward pairing, and post-backward pairing test trials to properly align odor delivery with neural responses.

Conditioning of flies in the closed loop system

The intersectional driver MB042B was used to express UAS-ChrimsonR.mCherry in the PAM dopaminergic cluster. For conditioning, ChrimsonR activation was performed by 1 s constant illumination of 565 nm (CoolLED, PE-100) light of approximately 150 $\mu W/mm^2$ intensity directed at the brain of the fly through the microscope objective. The LED was triggered using Prairie View software.

Tethered animals expressing UAS-ChrimsonR.mCherry in PAM neurons and LexAOP-GCaMP6s in the γ4 MBON were placed on an air-supported foam ball under the two-photon microscope and allowed time to acclimate until consistent walking was initiated. Each fly then experienced 3-4 full training paradigms consisting of a baseline trial, a forward-paired conditioning trial (ACV was presented for 10 s with LED illumination during the last second), a post-FP test trial, a backward-paired conditioning trial (DANs were activated for 1 s using LED illumination and then 1 s later a 10 s ACV presentation), and a post-BP test trial. The delay between the end of a conditioning trial and start of a testing trial was 40 s.

The difference in upwind position from ACV onset and ACV offset was used to calculate the upwind displacement of the fly in the odor presentation. The upwind displacement in clean air was also measured for the 10 s prior to each odor presentation to control for odor-independent modulation in behavior. If behavioral tracking was dropped by FicTrac at odor onset or offset, the behavioral analysis of upwind displacement for that odor presentation was excluded from the analysis. The change in upwind displacement after forward and backward pairing was measured by subtracting the mean upwind displacement in the odor trials preceding forward pairing or backward pairing from the odor trials immediately following conditioning. Likewise, the change in the γ4 MBON response after forward and backward pairing was measured by subtracting the mean odor-evoked GCaMP response in odor trials preceding forward pairing or backward pairing from the mean response in odor trials immediately following conditioning. A 500 ms delay was introduced to both measurement of upwind displacement and peak neural response to account for the lag in odor delivery from the odor vial to the antennae of the animal. The behavioral and neural modulation were plotted for each of the 3-4 training paradigms per animal to examine trial-to-trial variability (Figures 4F, gray dots, and S5B, S5D, and S5G). In addition, the mean of trials during the 3-4 training sessions per animal were analyzed to examine animal-to-animal variability (Figures 4C–4F, black dots, and S5A, S5C, and S5F).

Immunohistochemistry

Day 1 adult brains were dissected in Schneider's media (Sigma) then immediately transferred to cold 1% PFA (Electron Microscopy Sciences) and fixed overnight at 4°C. Following overnight incubation samples were washed in PAT3 Buffer (0.5% BSA/0.5% Triton/1X PBS pH 7.4) 3 times. Brains were blocked in 3% Normal Goat Serum for 90 minutes at RT. Primary antibodies 1:2000 rabbit anti-DAMB (Figure S7B) (a gift from Ronald Davis) (Feng et al., 1996), 1:20 guinea pig anti-DopR (Figure S7B) (Lebestky et al., 2009), 1:1000 chicken anti-GFP (Abcam ab13970) (Figure 1A) and 1:50 mouse anti-brp (Developmental Studies Hybridoma Bank nc82) (Figure 1A) were incubated 3 hours at RT then 2-3 days at 4°C. Brains were washed extensively in PAT3 Buffer. Secondary Alexa Fluor antibodies (Life Technologies) were incubated 3 hours at RT then 2-3 days at 4°C. Brains were washed 3 times in PAT3 Buffer then once in 1X PBS. Samples were mounted in Vectashield (Vector Laboratories). Images were captured on a Zeiss LSM 880 using a Plan-Apochromat 20X (0.8 NA) objective.

RNA Isolation and qRT-PCR

(Figure S7B)

Total RNA was isolated from the dissected brains of eight 1-day-old adult wild-type and DopR1$^{-/-}$ females. RNA was extracted using Qiazol reagent (QIAGEN) then column purified by RNeasy micro kit (QIAGEN). cDNA was generated using Quantitect Reverse Transcriptase kit (QIAGEN). Taqman real-time qPCR experiments were performed on a QuantStudio 12K Flex Real-Time PCR System (Thermo Fisher Scientific) following the manufacturer's instructions. Data were analyzed using the comparative 2ΔΔCt method using alphaTub84B as an endogenous control. The average fold-change relative to wild-type was calculated. The following Taqman assays from Life Technologies were used: *alphaTub84B* (Dm02361072_s1) and *DopR1* (Dm02134814_m1).

Experimental Design

The experimenter was not blinded to animal genotypes. All behavioral experiments were performed across multiple days. To control for any variation in chamber construction, a given genotype was assessed using different chambers located at different positions in the behavioral apparatus. Experimental and control genotypes were collected in parallel. For functional experiments, receptor mutant genotypes and drug treatment conditions were interleaved when applicable. To control for trial history, the order of inter-stimulus intervals tested in an independent sample in Figures 5A–5D, S6A–S6C, 6A–6D, and S7C were varied across experiments. No statistical methods were used to predetermine sample size.

QUANTIFICATION AND STATISTICAL ANALYSIS

Statistical analysis was performed using Prism and MATLAB with Bonferroni correction to p values when multiple comparisons were performed. The Shapiro-Wilk normality test was used to assess normality across all individual experiments. If the null hypothesis was rejected, Wilcoxon match-pairs signed rank or Mann-Whitney tests were used to compare for differences between two groups; otherwise, paired or unpaired t tests were used. All tests were two-tailed. Ordinary one-way ANOVA was used to test for differences across the three genotypes of wild-type, DopR1$^{-/-}$, and DopR2$^{-/-}$ animals in locomotor parameters and odor tracking behavior (Figures S8F–S8S). A RM one-way ANOVA with Geisser-Greenhouse correction was used to test for differences in DAN activation, VMAT release, and extracellular dopamine levels between FP, BP, and DAN activation (Figures S6A–S6C). One-sample t-tests or Wilcoxon signed-rank tests against zero were used to assess the significance of changes in KC- or odor-evoked responses in the γ2, γ4, and γ5 MBONs (Figures 2E, S3C–S3E, and 4E), behavioral modulation after conditioning trials (Figures 1F, 1G, S1E, 4C, and 4D), and changes in cAMP and ER-calcium levels in KC axons during conditioning (Figure 5E). Spearman's rank correlation was used to measure the correlation between changes in upwind displacement in odor and the change in odor-evoked calcium responses in the γ4 MBON across individual trials or averages for each animal (Figures 4F). The sample size for each experiment is indicated in the corresponding figure legend. For behavioral chamber experiments, the number of experiments is indicated in the figure legend and the number of flies used across all experiments can be found in the corresponding methods section. For functional imaging experiments, individual flies were treated as independent samples except in some explant experiments in Figures S3C and S3D where each hemisphere of the brain was treated as an independent sample and in Figures 4F and S5B, S5D, and S5G where each of the 3-4 conditioning trials for each animal across all 8 animals are plotted independently to show trial-to-trial variability (noted in figure legend).

DATA AND CODE AVAILABILITY

Customized MATLAB and Python scripts, C software, CAD files, and data in this paper are available upon request to the Lead Contact.

Cell

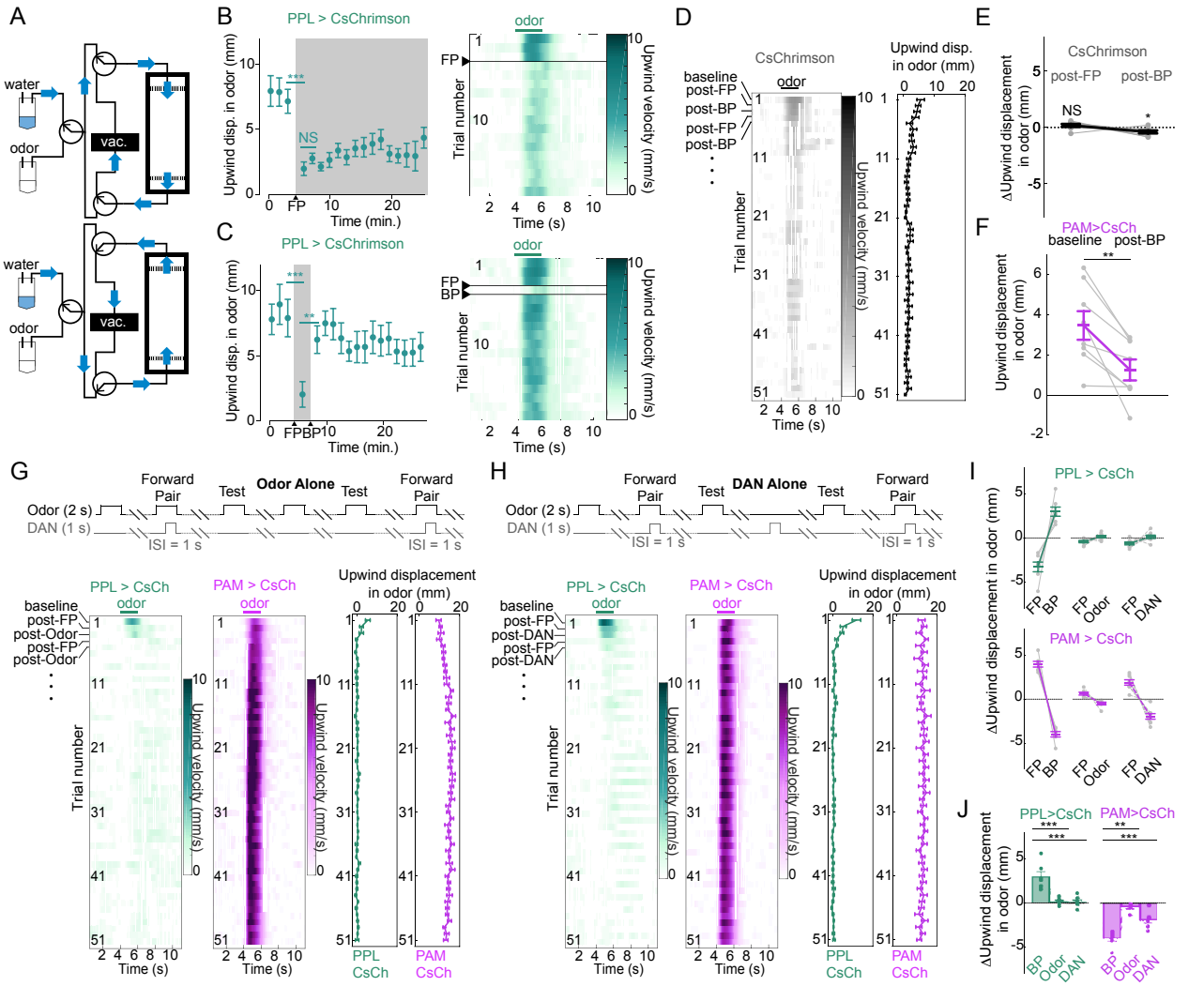

Figure S1. Forward and Backward Conditioning Drives the Formation of Opposing Olfactory Associations, Related to Figure 1

(A) Schematic of odor tracking chamber assay showing airflow switch across manifolds between odor presentations.

(B) Left: Mean upwind displacement for flies in apple cider vinegar (ACV) odor during 3 baseline trials and 15 trials following a single forward pairing (FP) of ACV with optogenetic activation of PPL > CsChrimson animals (post-FP trials highlighted in gray). Right: Raster of mean upwind velocity of flies for the corresponding trials.

(C) Same as in (B) except after a single post-FP trial, flies subsequently experienced a single backward pairing (BP). Paired t test with Bonferroni correction: ***p $\leq$ 0.001, ** $\leq$ 0.01, NS $\geq$ 0.05. For (B-C) n = 11 experiments; black arrowheads mark time when FP and BP was performed.

(D) Raster plot of mean upwind velocity of flies (left) and upwind displacement (right) using the same protocol as in Figure 1B except using CsChrimson flies lacking a Gal4 driver.

(E) Change in odor-evoked upwind displacement after FP and BP using CsChrimson flies lacking a Gal4 driver. n = 8 experiments. One-Sample t test against zero with Bonferroni correction: *p < 0.05, NS $\geq$ 0.05.

(F) Upwind displacement in ACV odor comparing baseline naive odor attraction and attraction following a single backward pairing (post-BP) trial of odor paired with optogenetic activation of PAM > CsChrimson animals, n = 8 experiments. Paired t test: **p $\leq$ 0.01.

(G) Top: Protocol for training was the same as in Figure 1B except instead of alternating forward and backward pairing, flies experienced alternating forward pairing and 2 s re-exposure to ACV (Odor Alone) during the training trial.

(H) Top: Protocol for training was the same as in to Figure 1B except instead of alternating forward and backward pairing, flies experienced alternating forward pairing and 1 s LED illumination used to re-activate DANs expressing CsChrimson (DAN Alone). Bottom (G-H): Mean raster plot of upwind velocity of flies (left) and upwind displacement in odor (right). PPL > CsChrimson (CsCh) shown in teal; PAM > CsCh shown in magenta.

(I) Mean change in upwind displacement comparing behavioral modulation resulting from alternating forward pairing (FP) and backward pairing (BP); or alternating forward pairing (FP) with re-exposure to odor alone (Odor); or alternating forward pairing (FP) with DAN stimulation alone (DAN) for PPL > CsChrimson and PAM > CsChrimson flies.

(J) Re-exposure to odor alone (Odor) or DAN alone (DAN) lead to weaker modulation of behavior than backward pairing (BP) for both PPL > CsChrimson (teal) and PAM > CsChrimson animals (magenta), n = 7-8 experiments. Mann-Whitney test with Bonferroni correction: ***p $\leq$ 0.001, ** $\leq$ 0.01. All data represent mean ± SEM.

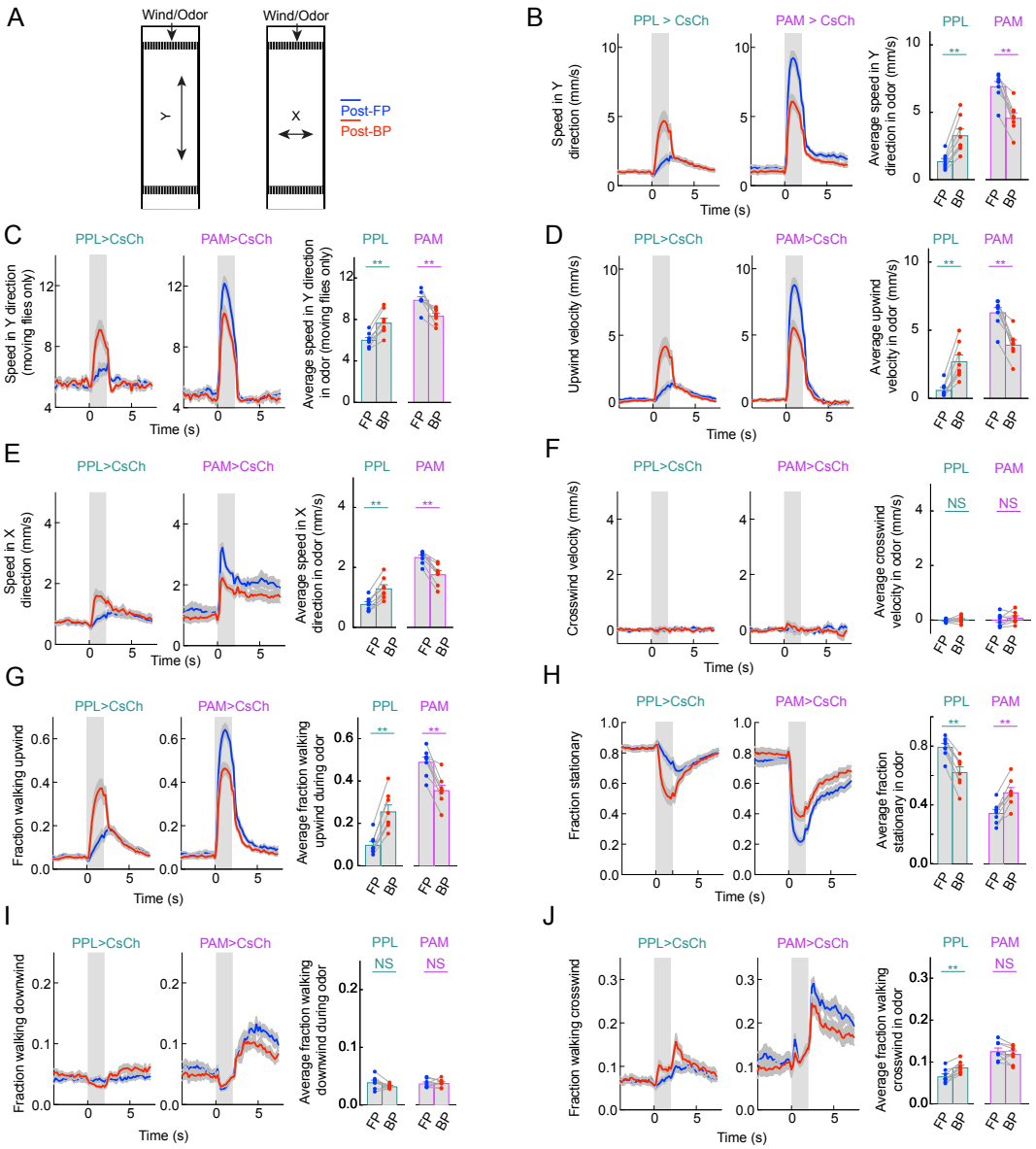

Figure S2. Forward and Backward Conditioning Modulates Multiple Aspects of Behavior, Related to Figure 1

(A–J) Multiple behavioral metrics are altered by forward pairing (post-FP) and backward pairing (post-BP) in PPL > CsChrimson (CsCh) and PAM > CsChrimson (CsCh) flies (same experiments as shown in Figures 1B–1G). For each panel, traces at left represent mean behavior over the duration of trial (time of odor stimulus denoted by gray box). Graphs at right quantify mean behavioral response in the odor. FP and BP represent behavior in trials after forward pairing and backward pairing respectively.

(A) Schematic of chamber with the definition of X and Y axis relative to the direction of the air/odor flow shown.

(B) Speed in the Y direction (upwind or downwind movement) for all flies.

(C) Speed in the Y direction for only flies walking.

(D) Upwind velocity for all flies.

(E-F) Speed in the X direction (movement left or right within the chamber) (E) and crosswind velocity for all flies (F).

(G) Fraction of flies walking upwind.

(H) Fraction of flies stationary.

(I) Fraction of flies walking downwind.

(J) Fraction of flies walking crosswind. Flies were considered walking (not stationary) when their speed was > 1 pixel/s or 0.3 mm/s, n = 8 experiments. See STAR Methods for details of behavioral analyses. Wilcoxon match-paired sign rank test: **p $\leq$ 0.01, NS $\geq$ 0.05. All data represent mean ± SEM.

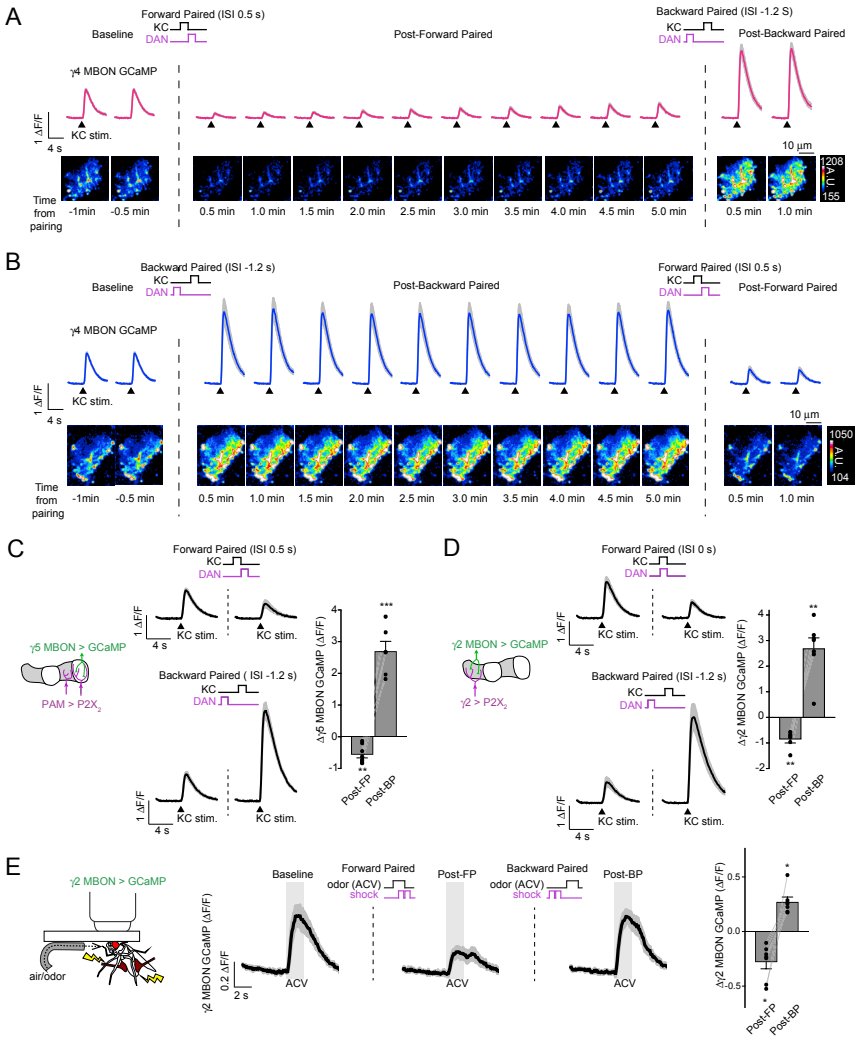

Figure S3. Relating Behavioral and Neural Modulation, Related to Figure 2

(A) Mean KC-evoked GCaMP6s response in the γ4 MBON prior to and after forward pairing (ISI = 0.5 s) or backward pairing (ISI = −1.2 s) using the same mushroom body explant preparation shown in Figure 2C. Two baseline trials are shown prior to forward pairing of KC and γ4 DAN activation. Following forward pairing (indicated by first dashed line), 10 responses to KC stimulation are shown prior to backward pairing (indicated by second dashed line). Two KC-evoked calcium responses in γ4 MBON are shown after backward pairing, n = 6 flies. Black arrowheads mark times of KC stimulation by iontophoresis of acetylcholine into the calyx. DANs expressed $P2X_2$ and were activated by iontophoresis of ATP. Below: Heatmap of fluorescence changes in γ4 MBON dendrites evoked by KC stimulation for each time point from a representative experiment (maximum intensity).

(B) Same as in (A) except backward pairing was performed first and forward pairing was performed second n = 6 flies. Black arrowheads mark times of KC stimulation.

(C) KC-γ5 MBON signaling is bidirectionally modulated by forward and backward pairing. Left: γ5 MBON responses to direct KC stimulation (black arrowhead) prior to (left) and after (right) forward pairing (ISI = 0.5 s, n = 8 MBONs, 7 flies) and backward pairing (ISI = −1.2 s, n = 6 MBONs, 6 flies) of KC and γ5 DAN activation. Right: Change in KC-evoked γ5 MBON response post-forward pairing (post-FP) and post-backward pairing (post-BP).

(D) Same as in (C) except for γ2 MBON responses prior to (left) and after (right) forward pairing (ISI = 0 s, n = 6 MBONs, 4 flies) and backward pairing (ISI = −1.2 s, n = 7 MBONs, 7 flies) of KC and γ2 DAN activation. One-sample t test against zero with Bonferroni correction: ***p ≤ 0.001, ** ≤ 0.01.

(E) Left: Schematic for conditioning fly with apple cider vinegar (ACV) odor and electric shock. Middle: Odor-evoked responses in the γ2 MBON during baseline, post-FP, and post-BP performed sequentially within the same animals. Right: Change in odor-evoked calcium response in γ2 MBON post-FP and post-BP, n = 7 flies. Signed Rank Test against zero with Bonferroni correction: * < 0.05. All data represent mean ± SEM.

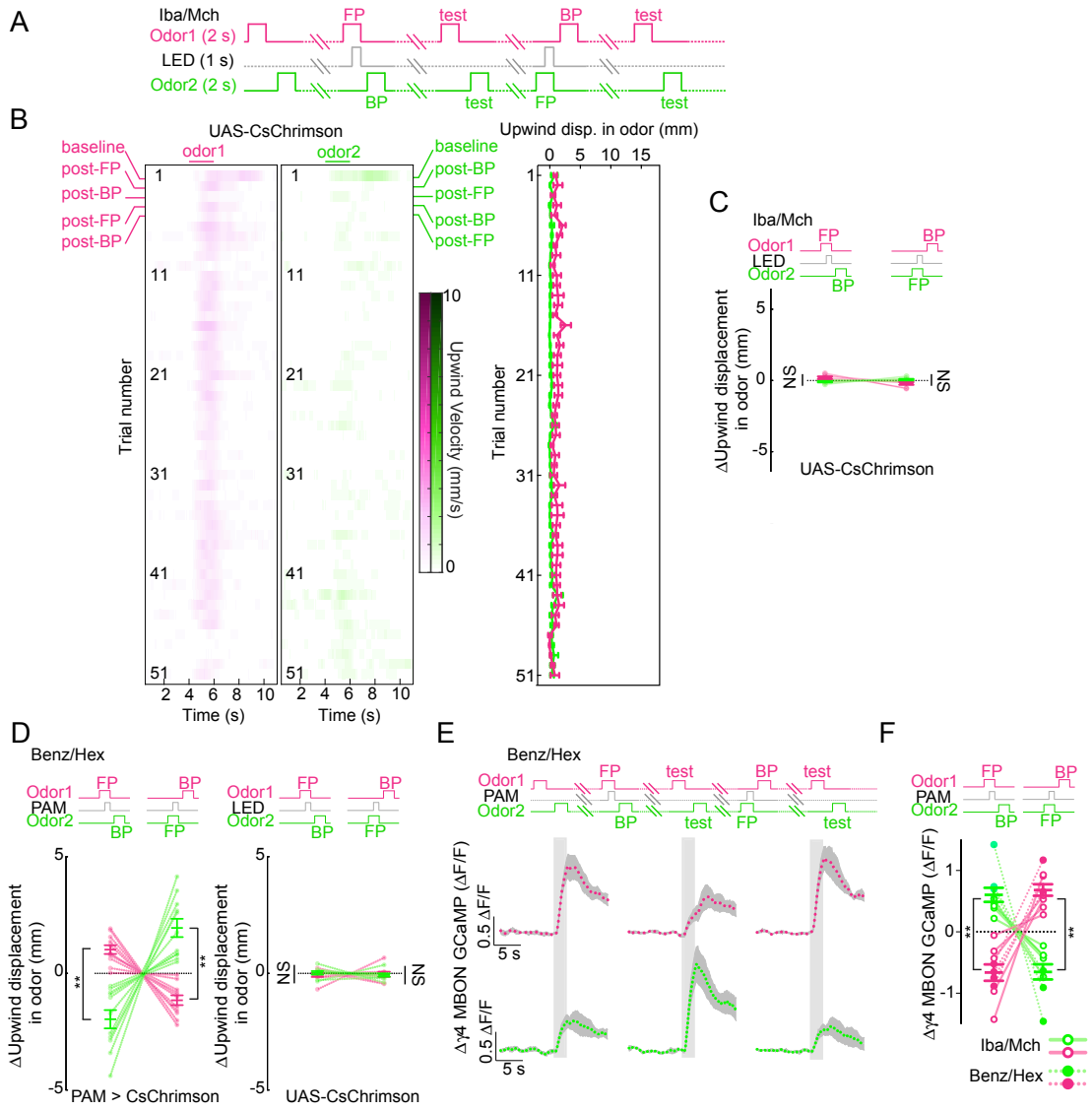

Figure S4. A Single Reinforcement Instructs Multiple Olfactory Associations, Related to Figure 3

(A) Behavioral training protocol, same as in Figure 3A (Odor1 is isobutyl acetate: Iba; Odor2 is 4-methylcyclohexanol: Mch).

(B and C) Same analysis as in Figures 3B and 3C except using CsChrimson flies, n = 7 experiments. Paired t test with Bonferroni correction: NS $p \geq 0.05$.

(D) Same behavioral protocol as in Figure 3A and analysis as in 3C except using different odors. Odors used were benzaldehyde (Odor1, Benz) and 1-hexanol (Odor2, Hex). Left: PAM > CsChrimson flies, n = 11 experiments. Right: Control CsChrimson flies, n = 9 experiments. Wilcoxon match-paired sign rank test with Bonferroni correction: $^{**}p \leq 0.01$, NS ≥ 0.05.

(E) Examining changes in γ4 MBON after training with two odors and a single DAN reinforcement as in 3F except the two odors used were benzaldehyde (Benz) and 1-hexanol (Hex), n = 4 flies.

(F) Change in γ4 MBON response to Odor1 (pink) and Odor2 (green) after Odor1 was forward paired and Odor2 backward paired (left points) and after Odor1 was backward paired and Odor2 forward paired (right points). Open circles: Data using Iba and Mch odor pairs (5 flies). Closed circles: data using Benz and Hex odor pairs (4 flies). Wilcoxon match-paired sign rank test with Bonferroni correction: $^{**}p \leq 0.01$. All data represent mean ± SEM.

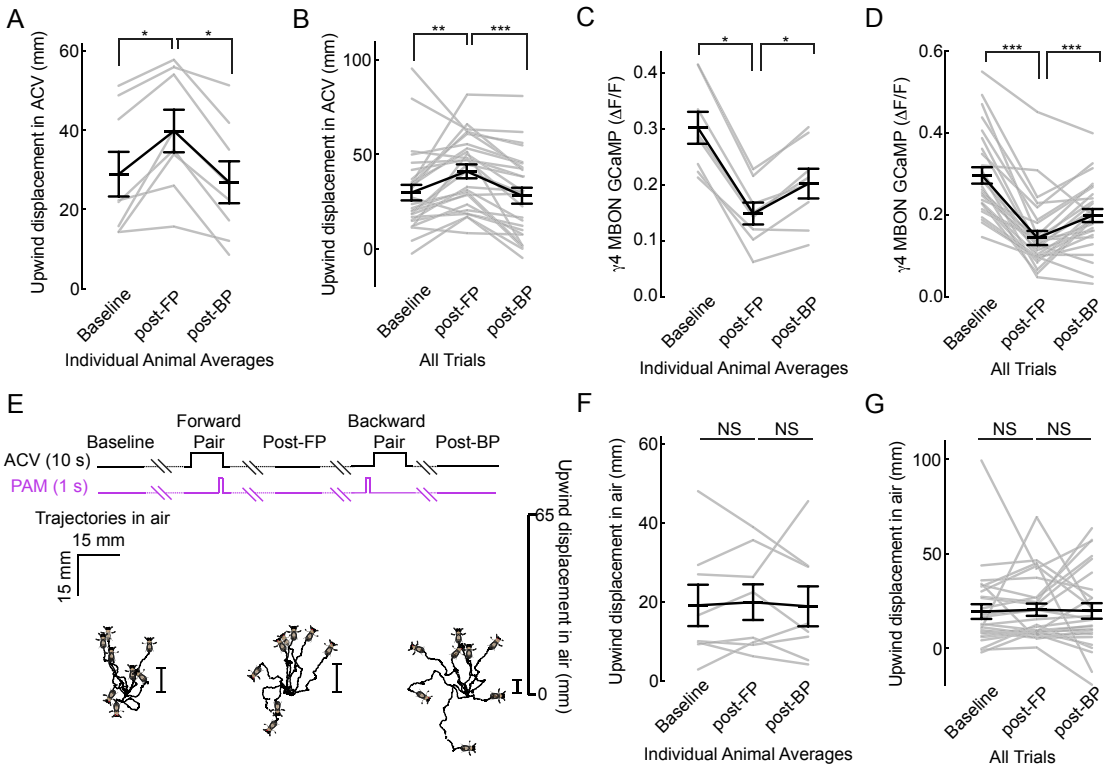

Figure S5. Synchronous Recordings of Neural and Behavioral Plasticity in Individual Flies, Related to Figure 4

(A) Mean upwind displacement in 10 s apple cider vinegar (ACV) odor during baseline, post-forward pairing (post-FP), and post-backward pairing (post-BP) trials, n = 8 flies. Each gray data point represents the mean upwind displacement across 3-4 conditioning protocols performed in an individual animal.

(B) Same as in (A) except for all training trials, n = 27 training trials across same 8 flies.

(C) Mean odor-evoked γ4 MBON responses in baseline, post-FP, and post-BP trials for the same 8 flies.

(D) Same as in (C) except for all training trials, n = 27 training trials across same 8 flies.

(E) Fictive 2D trajectories for representative individual fly (same as shown in Figure 4B) but for the 10 s prior to odor stimulation when animal was walking in a clean air stream.

(F) Same as in (A) except plotting mean upwind displacement in 10 s clean air prior to odor.

(G) Same as in (B) except mean upwind displacement in 10 s clean air prior to odor. Wilcoxon matched-pairs signed rank test with Bonferroni correction: ***$p \leq 0.001$, ** ≤ 0.01, * < 0.05, NS ≥ 0.05. Data are from the same flies as in Figure 4. All data represent mean ± SEM.

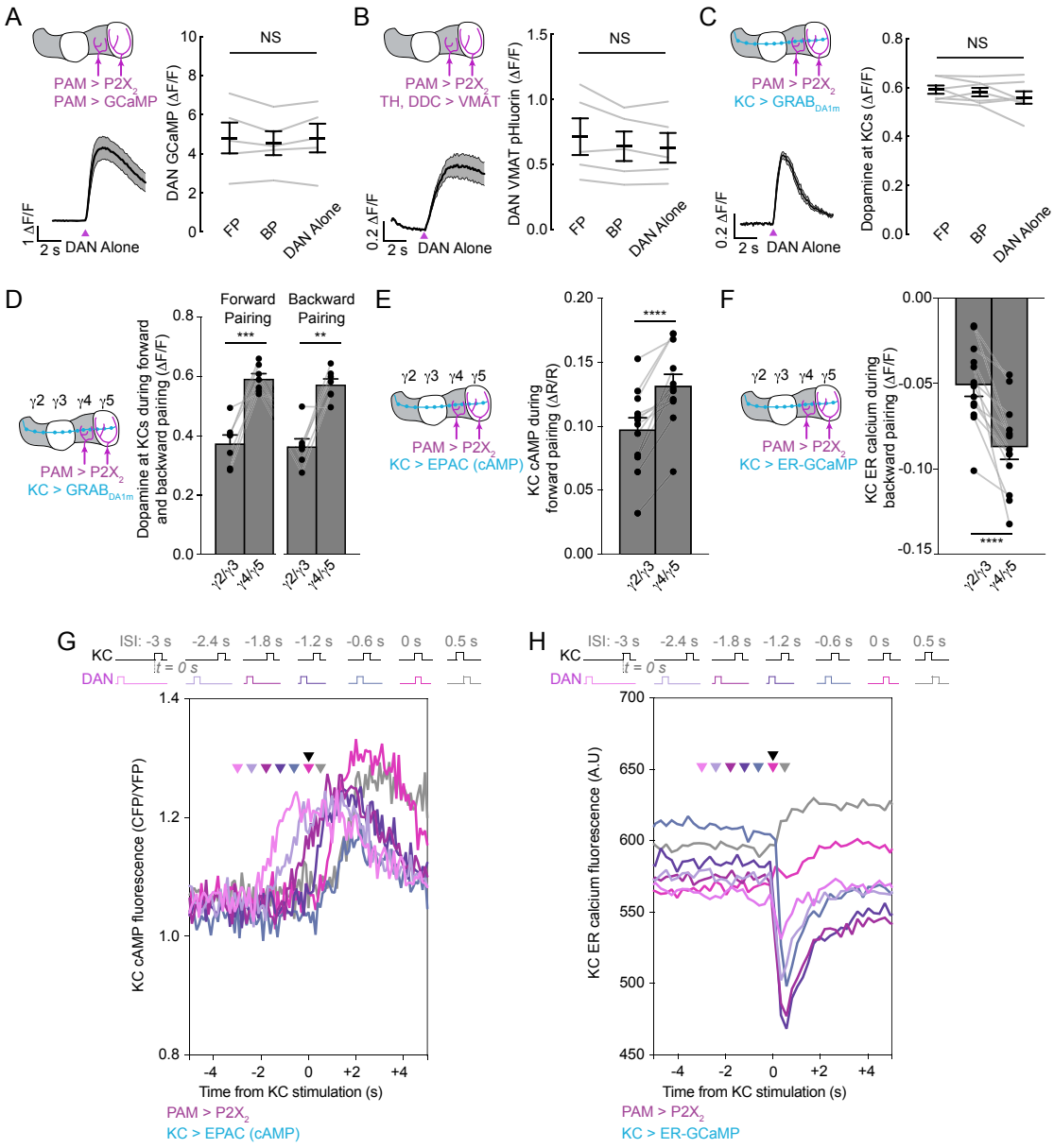

Figure S6. Second Messenger Pathways Are Sensitive to the Order of KC and DAN Input, Related to Figure 5

(A) GCaMP6s responses in γ4/γ5 DANs activated by ATP iontophoresis with co-expressed $P2X_2$ channel (left). Peak DAN calcium response during forward pairing (FP), backward pairing (BP) and DAN alone (right) n = 5 flies.

(B) VMAT-pHluorin fluorescence used to measure synaptic vesicular release from γ4/γ5 DANs activated by DAN stimulation (left). Peak fluorescent signal of VMAT-pHluorin from traces during FP, BP, and DAN alone (right), n = 5 flies.

(C) Dopamine sensor ($GRAB_{DA1m}$) expressed in KC axons and measured in the γ4/γ5 compartments during DAN stimulation (left). Peak fluorescent response of $GRAB_{DA1m}$ signal during FP, BP, and DAN alone (right), n = 7 flies. For (A-C) magenta arrowheads mark DAN stimulation. RM one-way ANOVA with Geisser-Greenhouse correction: NS $p \geq 0.05$.

(D) Comparison of dopamine sensor ($GRAB_{DA1m}$) signal in KC axons measured in either the γ2/γ3 or γ4/γ5 compartments where PAM DANs were directly stimulated, n = 7 flies. Data were re-analyzed from flies in Figure S6C.

(E-F) Comparison of cAMP (E) and ER-calcium release (F) in KC axon measured in either the γ2/γ3 or γ4/γ5 compartments; re-analysis of data from wild-type flies in Figures 5D, 6A, and 6C, n = 12 flies for cAMP and 13 flies for ER-calcium. (D-F) Paired t test: ****$p \leq 0.0001$, *** ≤ 0.001, ** ≤ 0.01.

(G) Representative CFP/YFP ratio in KC axons expressing EPAC sensor measured in the γ4/γ5 compartments during pairing of KC and DAN activation across 7 different ISIs used for conditioning.

(H) Representative ER calcium signal in KC axons expressing ER-GCaMP measured in the γ4/γ5 compartments during pairing of KC and DAN activation across 7 different ISIs used for conditioning. For (G-H) all traces were collected from the same preparation and aligned to the time of KC stimulation; black arrowhead marks KC stimulation, colored arrowheads mark DAN stimulation at indicated ISIs. All data represent mean ± SEM.

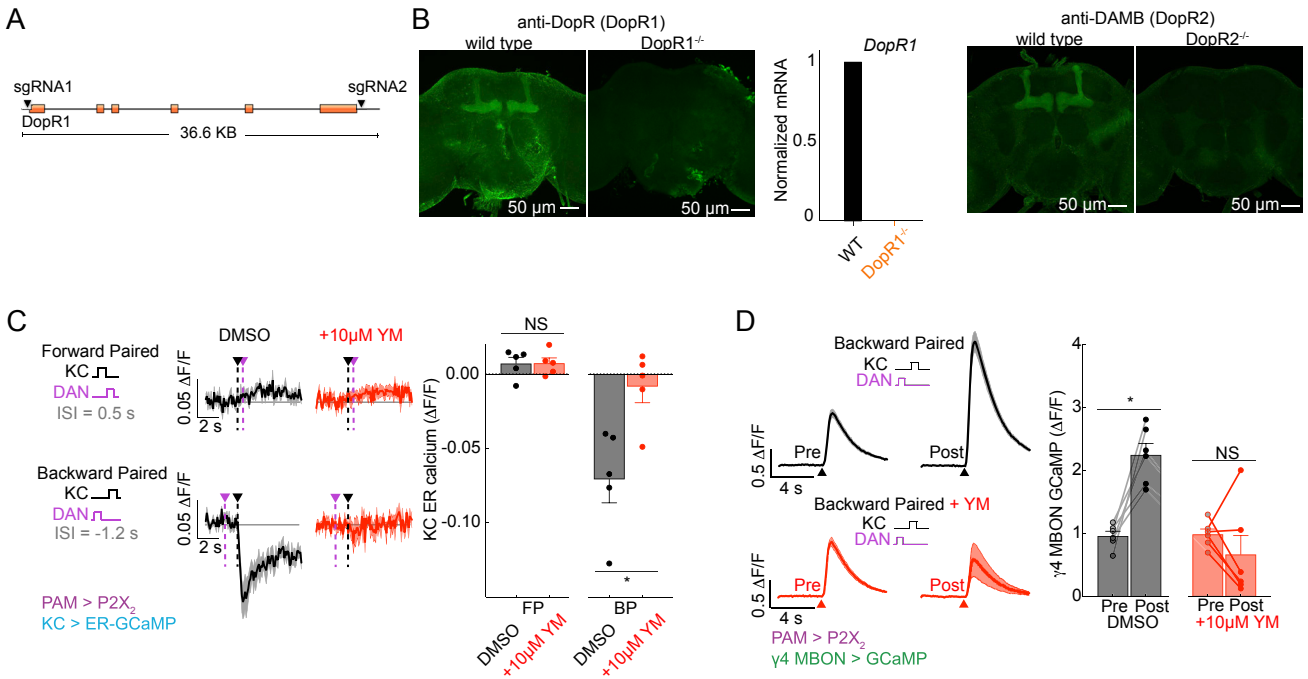

Figure S7. Distinct Roles of DopR1 and DopR2 in Second Messenger Production and Plasticity, Related to Figure 6

(A) Schematic of sgRNAs used to target Cas9 to the DopR1 locus. Orange boxes represent exons. sgRNA 1 targets the 5′ UTR and sgRNA 2 targets the 3′ UTR.

(B) Left: Immunohistochemistry with anti-DopR1 antibody in the adult brain of WT or DopR1$^{-/-}$ animals. RT-PCR confirming complete loss of *DopR1* mRNA in DopR1$^{-/-}$ mutant flies, RNA collected from 8 WT or 8 DopR1$^{-/-}$ brains and normalized to alphaTub84B. Right: Immunohistochemistry with anti-DopR2 antibody in the adult brain of WT and DopR2$^{-/-}$ animals. Maximum-intensity projection of Z stack.

(C) Left: Mean ER-GCaMP response in KC axon segments measured in the γ4/γ5 compartments during forward pairing (FP) and backward pairing (BP) in brain explant preparations bathed in 10 μM YM-254890, a Gaq inhibitor (red traces), or in DMSO control (black traces). Right: Mean ER-GCaMP response in KC axons in the presence (red) and absence (black) of 10 μM YM-254890 during FP and BP,n = 5 flies for each condition. Unpaired t test: *p < 0.05, NS ≥ 0.05. Black arrowhead marks KC stimulation, magenta arrowhead marks DAN stimulation.

(D) Left: Mean γ4 MBON GCaMP response to KC stimulation prior to and after backward pairing in brain preparations bathed in 10 μM YM-254890 (red) or in DMSO control (black). Black and red arrowheads mark time of KC stimulation. Right: Mean peak γ4 MBON response to KC stimulation prior to and after backward pairing in YM-254890 (red) or control (black), n = 6 flies for each condition. Wilcoxon matched-pairs signed rank test: *p < 0.05, NS ≥ 0.05. In (C-D) data represent mean ± SEM.

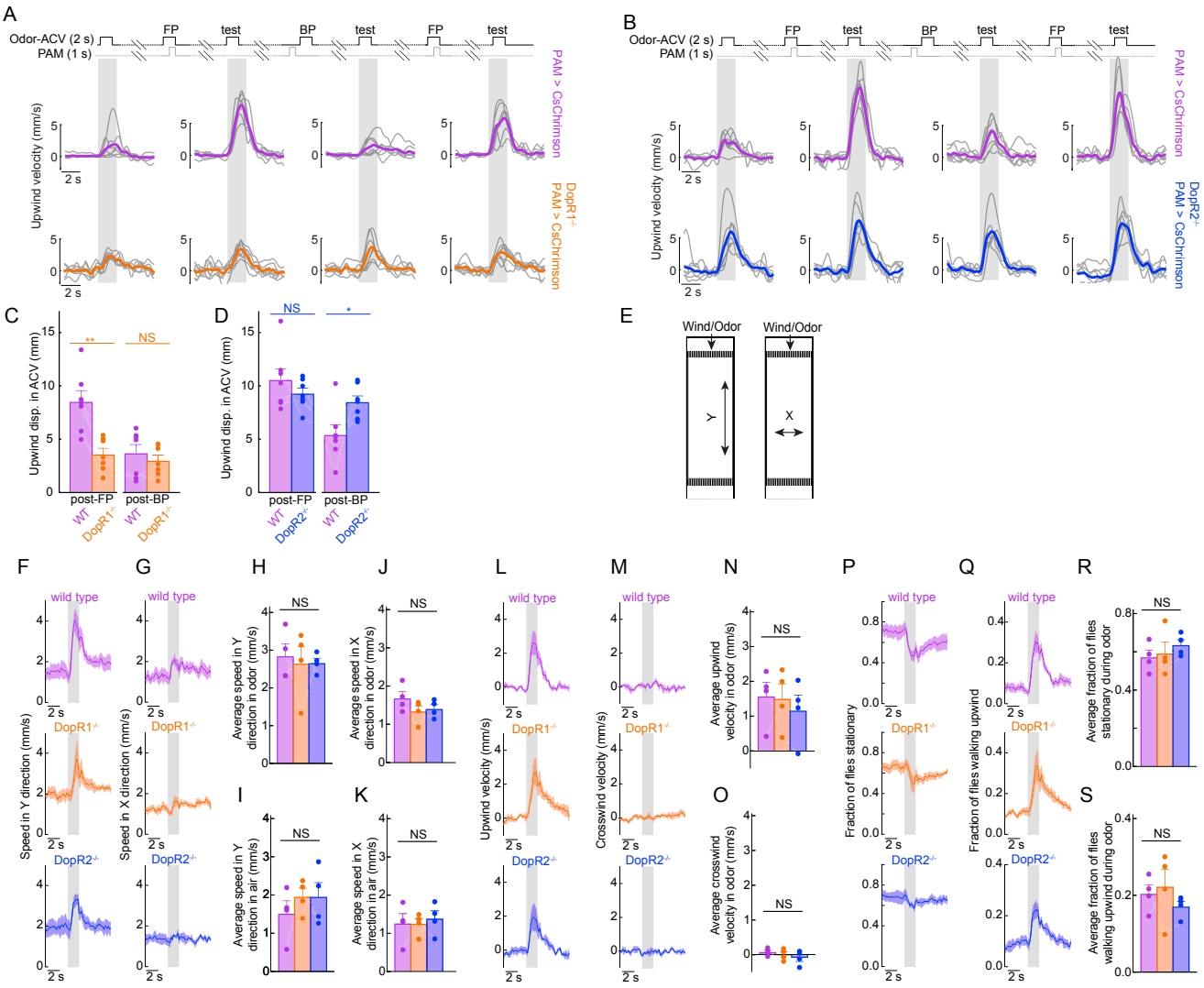

Figure S8. DopR1 and DopR2 Are Required for Behavioral Flexibility, Related to Figure 7

(A and B) Top: Protocol showing training with alternating forward pairing (FP) and backward pairing (BP) of apple cider vinegar (ACV) odor with PAM > CsChrimson. Bottom: Upwind velocity during the trials 7-10 (corresponding to trial number shown in Figures 7A and 7B) in wild-type (WT, magenta) and DopR1$^{-/-}$ (orange) flies (A) or WT (magenta) and DopR2$^{-/-}$ (blue) flies (B), n = 7 experiments. Individual experiments indicated by thin gray lines and mean indicated by bold colored line.

(C) Mean upwind displacement in odor post-FP and post-BP for WT and DopR1$^{-/-}$ flies.

(D) Same as in (C) except comparing WT and DopR2$^{-/-}$ flies. Unpaired t test: **p $\leq$ 0.01, * < 0.05, NS $\geq$ 0.05.

(E–S) Comparison of locomotor parameters in PAM > CsChrimson (CsCh) animals in a DopR1$^{-/-}$, DopR2$^{-/-}$, or wild-type (WT) background. Left: traces represent mean behavior over duration of trial; time of ACV odor stimulation indicated by the gray box. Right: graphs quantify mean behavioral response in air or odor, as specified by the axis label.

(E) Schematic of chamber with the definition of X and y axis relative to the direction of air/odor flow shown.

(F) Speed in the Y direction (upwind or downwind movement).

(G) Speed in the X direction (movement left or right).

(H and I) Average speed in Y direction during the 2 s of odor stimulation (H) or in the 4 s of clean air prior to odor presentation (I).

(J and K) Average speed in X direction during the 2 s of odor stimulation (J) or in the 4 s of clean air prior to odor presentation (K).

(L and M) Upwind velocity (L) and crosswind velocity (M).

(N and O) Average upwind (N) and crosswind velocity (O) in the odor.

(P and Q) The fraction of stationary flies (P) and flies walking upwind (Q).

(R and S) The mean fraction of stationary flies (R) and flies walking upwind (S) during odor presentation, n = 4 experiments. Ordinary one-way ANOVA: NS p $\geq$ 0.05. See STAR Methods for details in behavioral analysis. All data represent mean ± SEM.